2011

Antarctic sea ice carbon dioxide system and controls

Virginia Institute of Marine Science

Agneta Fransson
University of Gothenburg

Melissa Chierici
University of Gothenburg

Patricia L. Yager
University of Georgia

Walker O. Smith Jr.
Virginia Institute of Marine Science, wos@vims.edu

Antarctic sea ice carbon dioxide system and controls

Agneta Fransson,[1] Melissa Chierici,[2] Patricia L. Yager,[3] and Walker O. Smith Jr.[4]

Received 27 November 2010; revised 16 June 2011; accepted 16 October 2011; published 23 December 2011.

[1] In austral summer, from December 2008 to January 2009, we investigated the sea-ice carbon dioxide (CO_2) system and CO_2 controls in the Amundsen and Ross Seas, Antarctica. We sampled seawater, brine and sea ice for the measurements of total alkalinity (A_T), total inorganic carbon (DIC), pH, inorganic nutrients, particulate organic carbon (POC) and nitrogen (PON), chlorophyll a, pigments, salinity and temperature. Large variability in all measured parameters was observed in time and space due to the complex sea-ice dynamics. We discuss the controls of the sea-ice CO_2 system, such as brine rejection, biological processes, calcium carbonate ($CaCO_3$) precipitation/dissolution and CO_2 exchange. Most (80 to 90%) of the DIC loss was due to brine rejection, which suggests that the sea ice acted as an efficient DIC sink from 0.8 and 2.6 mol m^{-2} yr^{-1} (9.6–31 g C m^{-2} yr^{-1}). The remaining change in DIC was to a large extent explained by net biological production. The A_T:DIC ratio in the sea ice was higher than in the under-ice water (UIW), with ratios reaching 1.7, which indicated $CaCO_3$ precipitation and concomitant DIC loss in the sea ice. Elevated A_T:DIC ratios and carbonate concentrations were also observed in the UIW, which reflect the solid $CaCO_3$ rejected from the ice during melt. The potential for uptake of atmospheric CO_2 in the mixed layer increased by approximately 56 μatm due to the combined effect of $CaCO_3$ precipitation during ice formation, and ice melt in summer.

Citation: Fransson, A., M. Chierici, P. L. Yager, and W. O. Smith Jr. (2011), Antarctic sea ice carbon dioxide system and controls, *J. Geophys. Res.*, *116*, C12035, doi:10.1029/2010JC006844.

1. Introduction

[2] Ice-covered polar oceans are extremely sensitive to increased temperatures and increased oceanic CO_2 levels [*Stouffer et al.*, 1989; *Manabe et al.*, 1994; *Flato et al.*, 2000; *Orr et al.*, 2005]. The Southern Ocean (SO), in particular, is recognized as one of the most important regions for the marine carbon cycle, and its response to climate change, is predicted to have a large impact on atmospheric CO_2 [e.g., *Le Quéré et al.*, 2007; *Takahashi et al.*, 2009]. One major uncertainty within future predictions is the lack of data from the ice covered Southern Ocean; in addition, there is little agreement of the significance of the sea-ice cover in modulating CO_2 gas exchange. Biological production and CO_2 fluxes in the Southern Ocean are highly dependent on the ice cover and the formation and melting of sea ice [e.g., *Fransson et al.*, 2004; *Chierici et al.*, 2004]. Sea ice has previously been considered to be impermeable for gas exchange between ocean and atmosphere [e.g., *Yager et al.*, 1995; *Miller et al.*, 2002; *Fransson et al.*, 2004]. However, recent studies on gas fluxes between sea ice, ocean and atmosphere, conducted in ice-covered seas in both Antarctica and the Arctic have demonstrated that sea ice is permeable to CO_2, and that the sea-ice-air CO_2 fluxes should be reconsidered and included in regional and global carbon budgets [*Semiletov et al.*, 2004; *Nomura et al.*, 2006; *Delille et al.*, 2007; *Rysgaard et al.*, 2007; *Nomura et al.*, 2010a, 2010b; *Papakyriakou and Miller*, 2011]. Most experiments on sea-ice CO_2 fluxes have been performed in Arctic sea ice, with relatively few studies in Antarctic sea ice [*Ackley and Sullivan*, 1994; *Delille et al.*, 2007; *Lewis et al.*, 2010]. In the Weddell Sea during the Ice Station Polarstern (ISPOL) experiment, the focus was on the physical conditions for sea-ice-air gas transport, and it was found that gravity drainage and sea-ice bulk porosity were important in controlling gas exchange [*Tison et al.*, 2008].

[3] During the past two decades, the western Antarctic has experienced significant changes. Within this impacted region, the Amundsen Sea is one of the least studied areas due to its remote location, yet we know from satellites that the area has experienced significant surface warming and decreased summer sea-ice extent [*Stammerjohn et al.*, 2008]. Nearby glaciers, such as Pine Island Glacier [*Jacobs et al.*, 1996; *Jenkins et al.*, 1997; *Thoma et al.*, 2008] are also melting rapidly. In contrast, the Ross Sea shows increasing sea-ice extent and duration. The cause for these changes is likely

[1]Department of Earth Sciences, Oceanography, University of Gothenburg, Göteborg, Sweden.
[2]Department of Chemistry, Marine Chemistry, University of Gothenburg, Göteborg, Sweden.
[3]Department of Marine Sciences, University of Georgia, Athens, Georgia, USA.
[4]Virginia Institute of Marine Sciences, College of William and Mary, Gloucester Point, Virginia, USA.

0148-0227/11/2010JC006844

Table 1. A Summary of the Location, Sampling Date, Ice Thickness (h), and Snow Depth for Each Ice Station, Where Complete Ice Cores Were Sampled[a]

Station	UTC Date (Year-Month-Day)	Latitude (°S, dec)	Longitude (°W, dec)	Ice Thickness (cm)	Snow Depth (cm)	Slushy Layer (cm)	Free Board (cm)	Observation
1*	2008-12-12	70.65	107.01	100	32	3	–	Slush on top
2	2008-12-13	71.13	109.08	200	55	23	–	Porous snow stratification
6	2008-12-14	71.07	110.52	110	47	9	–	
13	2008-12-16	71.71	112.11	170	38	0	17	
16	2008-12-17	71.84	114.11	240	28	9	–	Stratified 76 cm
18*	2008-12-18	72.92	115.05	110	55			
21*	2008-12-20	72.60	116.02	113	5	n.d	–	
27	2008-12-21	72.42	115.96	290	47	7, 20–30	–	
33*	2008-12-22	71.92	118.38	125	60	18	–	Snowy ice top 57 cm
35*	2008-12-23	70.15	119.95	46	18	5	34	Snowy ice 8 cm top
36*	2008-12-26	69.41	125.38	97	36	6	–	No colored layer
37	2008-12-27	70.22	133.54	150	71	48	–	Strongly colored layer at 53 cm
38	2008-12-28	71.07	138.04	60	15	5	3	Snowy ice top 22 cm
39	2008-12-29	72.51	144.73	179	74	17	–	Snowy ice top 9 cm
40	2008-12-31	74.44	150.64	183	70	5	–	Top 28 cm colored
41*	2009-01-01	75.40	151.23	125	3	18, 40–60	–	Slushy core at several horizons

[a]For sea ice coverage and bottom topography at ice station locations, see Figures 1a and 1b. Stations included in the box model are marked with an asterisk. Dash denotes negative freeboard; n.d. means no data.

coupled to marine atmospheric forcing such as the Southern Annular Mode [*Stammerjohn et al.*, 2008]. Changes in sea-ice extent and the melting of glaciers affect the structure of the water column, sea-ice formation, and the marine ecosystem, which all have the capacity to induce changes in the ocean carbon uptake. The CO_2-system processes impacted during sea-ice formation and melt are not yet well understood and remain poorly quantified.

[4] The effect of biological processes on the variability of carbon transport within the sea ice is also little understood, but has a strong potential to affect the CO_2 transport and exchange with the surrounding environment. Sea ice forms a unique habitat for microorganisms such as algae, bacteria, and viruses, which are adapted to large changes in salinity, temperature, light, and nutrients [*Lizotte*, 2003; *Junge et al.*, 2004; *Thomas and Dieckmann*, 2010]. Algal biomass can reach substantial levels in some sea ice habitats [*Lizotte*, 2003], but the spatial distribution of sea ice algae is extremely discontinuous [*Dieckmann et al.*, 1998]. Sea-ice algae begin their growth earlier in the season than phytoplankton, presumably due to the stable irradiance environment provided by the ice. Previous observations have suggested that primary production by sea-ice algae accounts for up to 25% of the total primary production in the Southern Ocean, and potentially plays a significant role in the global carbon budget [*Arrigo and Thomas*, 2004]. In both the Arctic and Antarctic, studies have suggested that the organic carbon consumption by sea-ice heterogenic activity is high or higher in the melted sea ice than in the water below the sea ice [*Rysgaard et al.*, 2007; *Deming*, 2010, and references therein].

[5] During an opportunistic transect of Swedish Icebreaker *Oden* across the South Pacific sector of the Southern Ocean, we investigated the role of coastal Antarctic sea ice in the marine carbon cycle.

[6] The objectives of our study were 1) to describe the CO_2 system in Antarctic sea ice; 2) understand the quantitative relationships between physical, chemical and biological variables in Antarctic sea ice: 3) to investigate the controls that affect inorganic carbon in Antarctic sea ice; and 4) to investigate the potential uptake of atmospheric CO_2, using two different scenarios: with $CaCO_3$ precipitation within the sea ice and without, due to the combined effect of $CaCO_3$ precipitation in sea ice and dissolution during ice melt. In this work we contribute unique data on sea ice, under-ice water and brine from field measurements. Our study adds to the understanding of the intricate coupling between biogeochemical processes within the sea ice and chemical compounds of climatically significant gases in poorly investigated ice-covered Antarctic seas.

2. Study Area

[7] The Amundsen Sea is located between 69°S and 74°S along the Marie Byrd Land between 100 and 135°W. Due to its high concentrations of multiyear sea ice and remoteness from logistical bases, it has been one of the least studied continental shelf regions in the Southern Ocean. To the west and south is the better studied Ross Sea and its large open-water polynya [e.g., *Tremblay and Smith*, 2007]. Onboard the Swedish Icebreaker *Oden* during the Swedish-U.S. collaborative cruise *Oden Southern Ocean* 2008/2009 (OSO08–09), we sampled 16 stations (Table 1 and Figure 1) across this region for sea-ice cores, sea-ice brine, and seawater profiles. Our sampling occurred during the austral spring and summer 24-h sunlight period, between December 12, 2008 and January 1, 2009. Air temperatures ranged from −1.4° to −9.9°C and wind speeds from 5 to 25 m s^{-1}.

2.1. Sea Ice Cover and Extent

[8] The *Oden* broke through 50–100% ice cover and encountered sea-ice thicknesses up to about 3 m. At our stations, sea-ice thicknesses varied between 35–240 cm (rafted ice), with variable snow cover on top of the ice (Table 1). Snow depths ranged from 3–70 cm. Most of our stations exhibited a condition known as "negative freeboard," where the ice-snow surface is below sea level and flooded with seawater. Unlike thinner snow layers in the Arctic, thick Antarctic snow cover [*Thomas and Dieckmann*, 2010] acts to depress the snow-ice interface. We observed

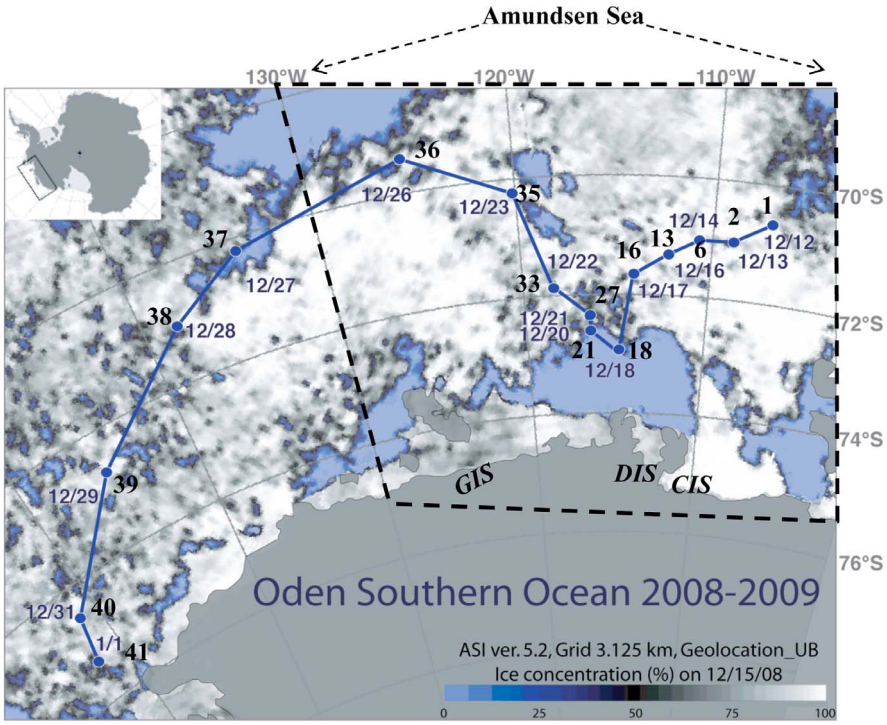

Figure 1. Mean sea-ice concentration for the December 2008 with cruise track for the Oden Southern Ocean expedition 2008/09 (blue line), sampling dates (blue dots), and station numbering. Blue areas show areas with no ice cover, and the polynya is clearly visible. The shaded gray area is area which is sea-ice covered. The area within box (dashed, black line) shows the limits of the Amundsen Sea. The land fast marine out-flowing glaciers along the coast are denoted; GIS for the Getz Ice Shelf; DIS, the Dotson Ice Shelf, and CIS marks the Crosson Ice Shelf.

slushy layers (described by *Perovich et al.* [2004]) ranging from 3–60 cm thick. We observed significant rafting and ridging on the thicker sea-ice floes. We also observed large areas of colored ice, so-called "brown ice" [*Ackley and Sullivan*, 1994]. In most of the individual cores, we found colored sections both at the top and in the upper to middle part of the cores (from 30 to 80 cm from top, Table 1), suggesting the presence of biological activity.

[9] We used the remotely sensed observations from 2008 to investigate the seasonal evolution of the sea-ice cover in the study area. Sea-ice concentrations in our study area were obtained from Advanced Microwave Scanning Radiometer (AMSR-E) daily sea-ice charts downloaded from the Webpage of the University of Bremen [*Spreen et al.*, 2008]. A dramatic change occurred from a nearly completely open Amundsen Sea at the end of February (Figure 2a), to maximum ice extent in August (Figure 2b), with few and small coastal polynyas to significant ice-free areas and open coastal polynyas in the Amundsen and Ross Sea again clearly visible in December 2008 (Figure 2c).

2.2. Hydrography

[10] The Amundsen Sea and Ross Seas both are influenced by polynyas (open areas in an otherwise sea-ice covered region), mainly caused by catabatic winds from the Antarctic continent and upwelling of relatively warm subsurface water. The inflow of warm Circumpolar Deep Water (CDW) carried by the Antarctic Circumpolar Current (ACC), largely influences the area, and has been the main cause for the increased rate of glacier melt [*Jacobs et al.*, 1996; *Thoma et al.*, 2008]. As the CDW is introduced onto the continental shelf, it mixes with the fresh and cold Antarctic Surface Water (AASW) to form Modified Circumpolar Deep Water (MCDW). In the Amundsen Sea the MCDW enters the shallow shelf along deep troughs [*Nitsche et al.*, 2007]. In our study area, along 114°W, MCDW is found at about 400 m with a temperature maximum and salinity >34.5 (Figures 3a and 3b). The relatively cold and fresh surface layer is due to the mixing of sea-ice meltwater and the cold winter water (WW) to form the Antarctic Surface Water (AASW). The WW is a remnant from winter and exhibits a temperature minimum between 50 and 100 m in our study (white dashed line in Figure 3a).

3. Methods

3.1. Sample Collection

[11] Bulk sea ice (hereafter referred to as sea ice), brine, and seawater were collected for the determination of total inorganic carbon (DIC), total alkalinity (A_T), pH, inorganic nutrients (phosphate, nitrate and silicate), chlorophyll *a* (chl), particulate organic carbon (POC) and nitrogen (PON), pigments, heterogenic respiration, salinity, and in situ temperature. Sea ice was collected using two different ice corers. Chemical measurements were made primarily on cores collected by a stainless steel barrel ice auger with polished steel cutting teeth (diameter of 0.12 m). Biological samples were collected using a Kovacs Mark V fiberglass coring

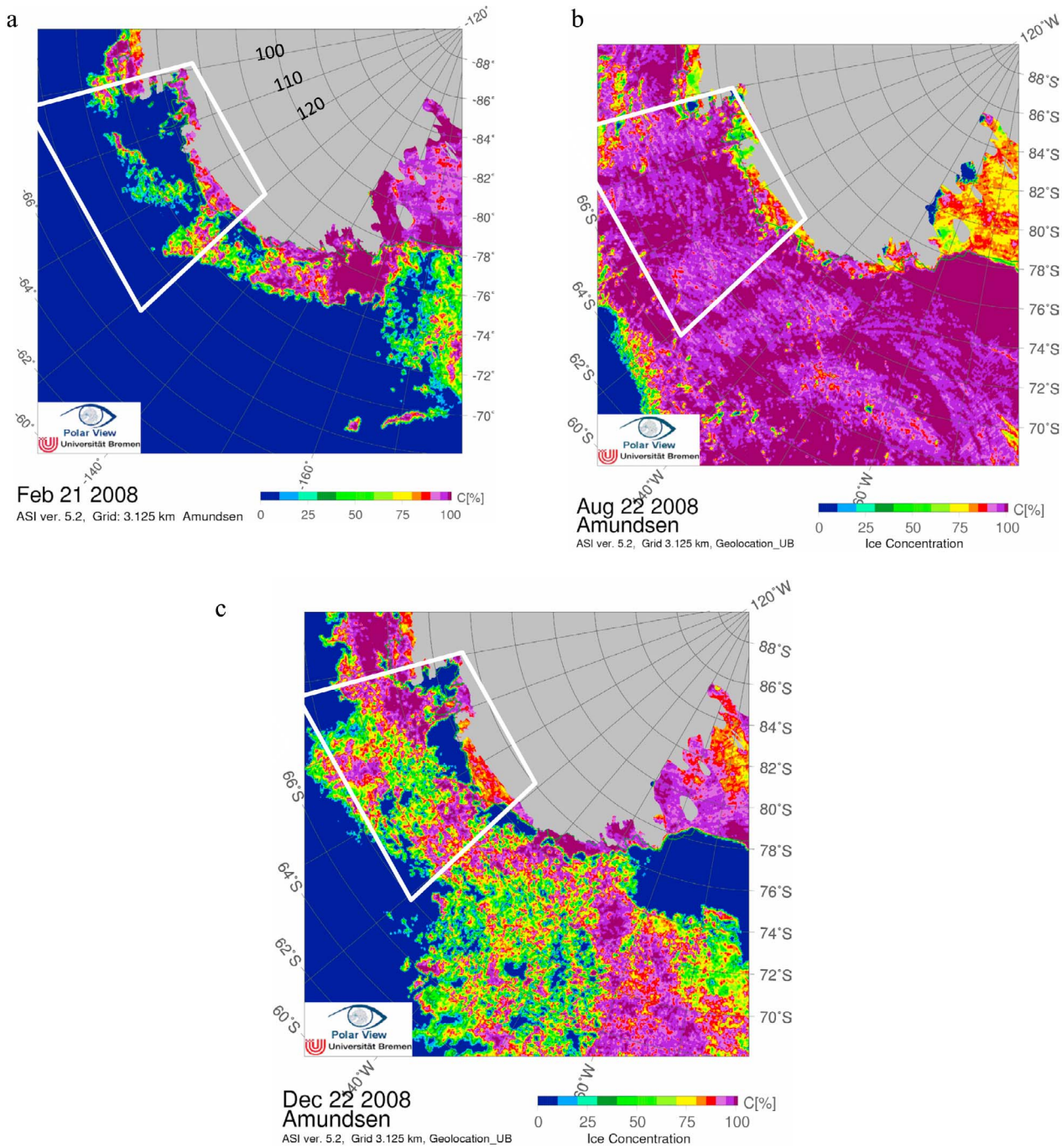

Figure 2. Mean daily sea-ice concentration from the Advanced Microwave Scanning Radiometer (AMSR-E) remotely sensed data in the study area during (a) 21st of February 2008, (b) the 22nd of August 2008, and (c) the 22nd of December 2008. The gray area denotes land, the dark blue areas show the open ocean, and the dark purple areas are areas with 100% ice concentration. The Amundsen Sea is the area within the white box. The daily sea-ice charts were downloaded from the Webpage of the University of Bremen, http://iup.physik.uni-bremen.de/iuppage/psa/2001/amsrop.html [*Spreen et al.*, 2008].

system (0.14 m diameter) with stainless steel cutting teeth. Sea-ice temperature was measured on site, immediately after the ice core was recovered, at 5-cm intervals using a digital thermistor (Amadigit) with the accuracy of 0.1°C. The holes for the temperature measurement were carefully drilled manually with a stainless steel hand-drill to avoid additional heating from the drill. The sea-ice core for chemical measurements was sliced with a clean stainless steel saw into 10–12 cm horizons, transferred to gas tight bags (Tedlar®) and immediately sealed, from which air was removed using a small vacuum hand pump (Nalgene®). Biological cores were similarly sliced into 10 cm horizons, transferred to

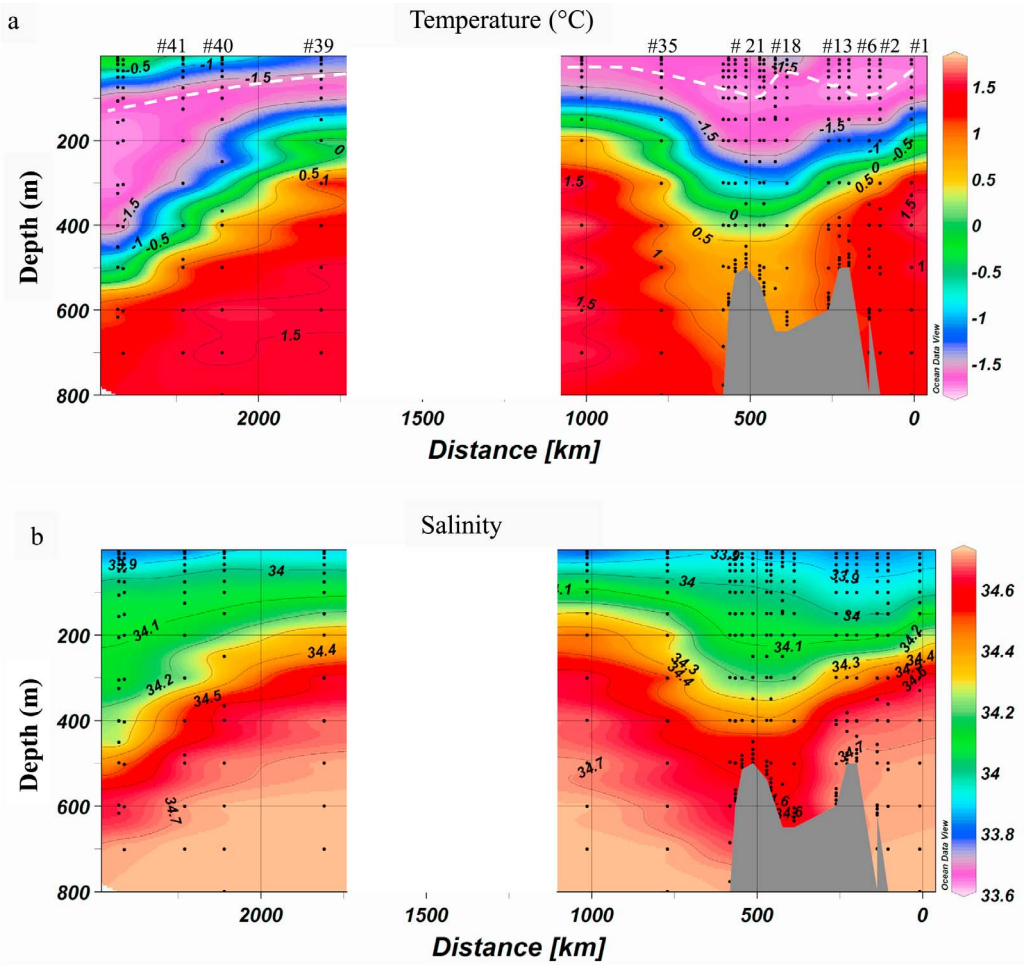

Figure 3. Section plots of distance (km) and (a) temperature (°C) and (b) salinity in the upper 800 m in the water column from station #1 in the northern end of the Amundsen Sea (right end) to station #41 in the Ross Sea. The white dashed line in the temperature plot denotes the depth of the temperature minimum, which defines the winter water (WW). White area in both plots shows the area of no data.

acid-washed plastic containers, and diluted to 50% with filtered seawater to prevent salinity shock upon melt. The samples were slowly melted in darkness at 15°C for approximately 24 h. At ice sampling, the thickness of slushy layer, sea-ice freeboard, and sea-ice core length were measured with a plastic measuring stick and visually investigated regarding stratification and color (Table 1). When the sea ice was not submerged, we collected brine in "sackholes" at different depths varying between 40 and 60 cm in the ice (Table 2a), after approximately 15 min, using a syringe for

Table 2a. Properties of the Brine Sampled From Sackholes Drilled at Depths Varying Between 40 and 60 cm in the Ice[a]

Station	Depth (cm)	T (°C)	S	DIC (μmol kg^{-1})	A_T (μmol kg^{-1})	A_T:DIC	fCO_2 (μatm)	$[CO_3^{2-}]$ (μmol kg^{-1})
2	40	−2.3	38.9	2006	2625	1.3	48	418
2	60	−2.3	37.9	2144	2548	1.2	99	273
13	40	−2.5	43.3	2143	2932	1.4	41	515
13	40	−2.5	42.9	2142	2900	1.3	43	536
16	60	−2.4	33.5	2191	2711	1.2	64	369
18*	60	−1.9	33.5	1979	2201	1.1	159	152
21*	40	−2.1	34.3	1463	2357	1.6	9	608
21*	60	−2.1	33	1451	2343	1.6	8	613
33	n.d	n.d	n.d	n.d	n.d	n.d	n.d	n.d
35	n.d	n.d	n.d	n.d	n.d	n.d	n.d	n.d
36*	40	−1.1	35.3	2204	2426	1.1	210	156
Average ± stdev		−2.1 ± 0.4	37 ± 4	1969 ± 300	2561 ± 254	1.3 ± 0.2	76 ± 69	404 ± 180

[a]The stations included in the model are marked with an asterisk; "n.d." denotes no data. The fugacity of carbon dioxide (fCO_2, μatm) and the carbonate ion concentration ($[CO_3^{2-}]$) were calculated using the CO2SYS program [*Pierrot et al.*, 2006]. The average and standard deviations (stdev) are calculated for each parameter and nine measurements.

gas samples to minimize the effect of gas exchange with the atmosphere. Larger volumes for biological samples were collected by a small hand pump into sterile glass bottles and kept cold and dark until processed. Before sampling, the sackholes were covered with a plastic lid to avoid CO_2 exchange with the atmosphere. Brine temperature (Table 2a) was measured with the digital thermistor in the brine sackholes on site, immediately after sampling. Snow depth was measured in the snow pit as the depth between the slushy layer and the snow surface (Table 1), using a measuring stick. Before CO_2-system analysis, the melted sea-ice samples were carefully transferred from the bags to borosilicate glass bottles (250 ml) using tubing to minimize contamination from the atmosphere, and thermostated to 15°C.

[12] For under-ice water sampling we used an electric submersible pump attached to a reticulate pole to allow for undisturbed sampling away from the actual hole, at approximately 0.1–0.2 m below the sea ice, into a borosilicate glass bottle with gas-tight lid, where we immediately measured water temperature. Collection of sub-surface seawater (greater than 5 m) profiles from the ship was co-located with the ice stations, and samples were collected following standard protocols [*Dickson et al.*, 2007] from 12-L Niskin bottles mounted on a General Oceanics 24-bottle rosette equipped with a Conductivity-Temperature-Depth sensor (CTD, Seabird SBE-911 plus).

3.2. Sample Processing

[13] A_T was determined by potentiometric titration in an open cell with 0.05 M hydrochloric acid (HCl), according to *Haraldsson et al.* [1997]. DIC was determined by gas extraction from acidified seawater samples, followed by coulometric titration with photometric detection [*Johnson et al.*, 1985, 1987; *Dickson et al.*, 2007]. The precision of the A_T and DIC measurements were obtained by triplicate analysis of one sample, and was estimated to ca. ±2 μmol kg^{-1} and ±1 μmol kg^{-1}, respectively. The accuracy of A_T and DIC was controlled against a certified reference material (CRM, batch #90) supplied by Andrew Dickson (Scripps Institution of Oceanography, San Diego, USA) at the beginning and at the end of 20 samples.

[14] pH was determined spectrophotometrically (Diode-array spectrophotometer, HP8452) using a 2 mM solution of the sulphonaphtalein dye, m-cresol purple, as an indicator [*Clayton and Byrne*, 1993]. Prior to analysis the samples were thermostated to 15°C. Samples were measured in a 1-cm flow cell, where the temperature was measured in the sample upstream of the flow cell using a thermistor (Pt 100). The analytical precision was estimated to ±0.002 pH units, which was determined by triplicate analysis of one sample every day. The pH of the indicator solution was measured daily using a 0.2-mm flow cell. The magnitude of the perturbation of seawater pH caused by the addition of the indicator solution was calculated and corrected for using the method described by *Chierici et al.* [1999]. The accuracy of spectrophotometric pH values is difficult to assess, since it relies ultimately on the physicochemical characteristics of the indicator solution. Commonly, the overall accuracy is determined by the accuracy of the temperature measurements and the accuracy in the determination of the equilibrium constants of the dye, which has been reported to be approximately ±0.002 pH units [*Dickson*, 1993].

[15] Samples for inorganic nutrients measurements in melted ice samples were filtered using GF/F glass filters (45 μm) under low pressure prior to analysis. Colorimetric determinations of phosphate (PO_4), nitrate (NO_3), and silicic acid ($Si(OH)_4$), were performed onboard the ship, immediately after melting of the sample, on an autoanalyzer using routine methods [*Grasshof*, 1999]. Salinity and conductivity of the melted sea ice, brine, and under ice water were measured using a conductivity meter (WTW Cond 330i, Germany) with a precision and accuracy of ±0.05. Salinity was also measured during DIC analysis by a calibrated SeaBird conductivity meter.

[16] Samples for pigment measurements were filtered through 25 mm GF/F filters. For determination of chlorophyll *a*, the filters were extracted in 90% acetone for 24 h in darkness (T = −10°C), and the resultant extract assessed using fluorescence [*United Nationals Educational, Scientific, and Cultural Organization*, 1996]. Accessory pigment samples were filtered through GF/F filters, frozen at −80°C, and returned to the laboratory for analysis by high performance liquid chromatography. Full details of the analytical techniques are provided by *Smith and Asper* [2001] and *Smith et al.* [2011]. Particulate carbon and nitrogen samples were filtered through precombusted (450°C for 2 h) GFF filters, placed in combusted glass vials and capped with combusted aluminum foil, dried at 60°C, and returned to the laboratory for analysis on a Carlo-Erba 1108 elemental analyzer using acetanilide as a standard [*Gardner et al.*, 2000]. Blanks were filters through which a few mL of filtered seawater had passed and were treated as above.

[17] For microbial community respiration rate measurements, under-ice seawater, brine, and biological ice core melt samples from highly colored layers each dispensed aseptically following collecting into six sterile, 200-ml pyrex bottles with ground glass stoppers, sealed, and incubated at −1°C in the dark. Pairs were fixed with 0.2% saturated mercuric chloride solution at 0, 24 and 48 h. Samples were processed shipboard for DIC as described above. Net heterotrophic respiration rate was calculated by linear regression through the six time points. Samples for bacterial abundance were also collected from initial samples, fixed with borate-buffered 2% formalin, and returned home frozen for processing on a flow cytometer [*Gasol and De Giorgio*, 2000].

[18] We used A_T and DIC, measured at 15°C, salinity and temperature together with the CO_2-calculation program CO2SYS [*Pierrot et al.*, 2006], to calculate fugacity of CO_2 (fCO_2), and carbonate ion concentrations [CO_3^{2-}]. We used the CO_2-system dissociation constants (K*1 and K*2) estimated by *Roy et al.* [1993, 1994], since an internal consistency study showed them to be the most suitable constants for cold and fresher surface waters [*Chierici and Fransson*, 2009]. The calculations were performed on the total hydrogen ion scale (pH_T) using the HSO_4^- dissociation constant of *Dickson* [1990]. An internal consistency check for the CO_2-system parameters was performed, comparing calculated DIC from A_T and pH with measured DIC. The linear regression (zero intercept) of 100 data points between the measured and calculated DIC gave a correlation coefficient (r^2) of 0.998, and the root mean standard deviation (rms) of ±11 μmol kg^{-1}. Due to the restricted number of data points of measured nutrient concentrations, we excluded

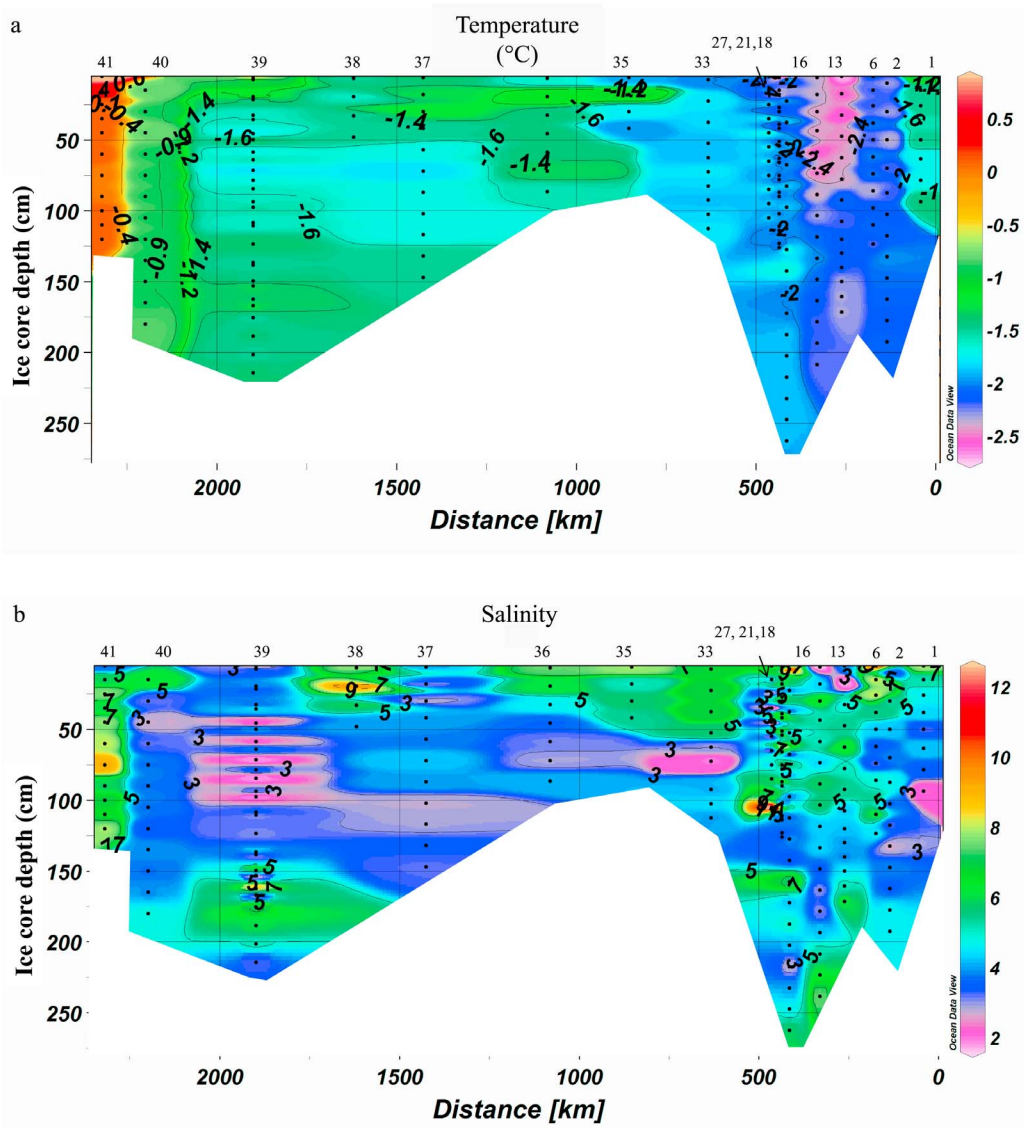

Figure 4. Variability in the sea-ice core (cm) of (a) temperature (°C) and (b) salinity, from station #1 (distance 0 km, right end) to station #41 (left end). Station numbers are shown at the top of the plot with reference to Figure 1 and Table 1 for location.

PO_4 and $Si(OH)_4$ in the CO_2-system calculations. Mean values of PO_4 and $Si(OH)_4$ in the bulk sea ice were 0.3 and 7.5 μmol L^{-1}, respectively. By not including PO_4 and $Si(OH)_4$, the calculated DIC differed on average by 0.4 μmol kg^{-1} and a relative error of 0.14% for a mean DIC value of 273 μmol kg^{-1}. All plots were compiled using Ocean Data View (R. Schlitzer, 2002, available at http://www.awi-bremerhaven.de/GEO/ODV).

4. Results and Discussion

4.1. Biogeochemical Properties of Sea Ice, Brine and Under-Ice Water

4.1.1. Variability of Temperature, Salinity and Physical Characteristics

[19] Table 1 summarizes information on the characteristics of the ice cores, such as sea-ice thickness, snow depth, slush layer, occurrence and depth of freeboard, and stratification. The measured parameters showed large variability across our study area (Figure 4), reflecting typical sea-ice heterogeneity and dynamics, differences in latitude, and our temporal sequence of sampling. The ice floes generally moved in a north-south direction due to the wind (data not shown). The northern stations (#35 and #36) were located close to the ice edge, in the vicinity of the Polar Front, and they were likely affected by warmer surface water and wave action.

[20] A common feature of Antarctic sea ice is deep snow cover, which was found in our study. Snow cover limits the irradiance to the ice and underlying water, affecting primary production and CO_2 uptake. The mean snow depth (and standard deviation) was 38 cm (±22 cm). Minimum snow depth of 3 cm was found at station Sta. 41 (#41), whereas Sta. #39 and #40 had the deepest snow layers of 74 and 70 cm, respectively (Table 1). Most of the stations had negative freeboard due to the snow weighing down the

Table 2b. Properties of the Under-Ice Water (UIW; Sampled From a Depth of 0.1 to 0.2 m Below the Sea Ice) of the Stations Included in the Model[a]

Station	T (°C)	S	DIC (μmol kg^{-1})	A_T (μmol kg^{-1})	A_T:DIC	fCO_2 (μatm)	$[CO_3^{2-}]$ (μmol kg^{-1})
1	−1.8	33.1	2282	2368	1.04	445	78
18	n.d	n.d	n.d	n.d	n.d	n.d	n.d
21	−1.8	33.4	2125	2296	1.08	234	123
33	−1.7	33.6	2163	2290	1.06	319	97
35	−1.7	33.3	2179	2274	1.04	395	80
36	−1.2	33.4	2181	2276	1.04	409	80
41	0.4	33.4	2174	2274	1.05	428	83

[a]The fugacity of carbon dioxide (fCO_2, μatm) and the carbonate ion concentration ($[CO_3^{2-}]$) were calculated using the CO2SYS program [*Pierrot et al.*, 2006]; "n.d." denotes no data.

snow-ice interface, causing flooding of the upper part of the sea ice. Flooding by seawater affects the properties of the ice, and consequently the processes controlling the CO_2 system.

[21] All ice cores, except Sta. #13, had a slushy layer between the top 5 and 20 cm, which at times had visible coloring by algal pigments. The ice core at Sta. #13 was the coldest, and covered with a dry, cold, and hard snow layer. Station #13 was also one of three stations with a positive freeboard of 17 cm. This suggests that seawater could not infiltrate the sides to form a slush layer at the snow-ice interface, protecting the sea ice from interaction with underlying seawater. The cores at Sta. #13 and #16 were stratified at several places in the core, and within these we noted a decrease in temperature and salinity, indicating a more frozen layer within the core. The thickest ice cores at Sta. #16 and #27 were likely due to rafting of floes soon after formation or ridging at a later stage.

[22] Individual sea-ice cores demonstrated a negligible vertical temperature gradient. The temperature varied between −2.8°C and +1°C in the top 10 cm (ice-snow interface) of the ice cores, and between −2.5°C and 0°C at the ice-water interface (Figure 4a). In this study, the coldest ice cores were found at Sta. #13 and #16 (Figure 4a), early in the season. Salinity (S) in the melted sea-ice samples varied from 1.8 to 10 in the top sections and from 2 to 13 in the bottom portions of the ice cores (Figure 4b). Salinity in most of the ice cores had a typical C-shaped distribution [e.g., *Malmgren*, 1927], with the highest S in the top 10 to 15 cm of the ice-snow interface, lowest at intermediate depth, and high S at the bottom (closest to the seawater). This pattern confirms that most of the sea ice in our study was first-year ice [e.g., *Malmgren*, 1927], and had not undertaken significant melting. However, in a few of the ice cores (Sta. #1, #21, and #41) the salinity deviated from the C-shape, and the ice was likely in a partly melted stage. Warmer ice cores showed lower S in the upper portion, which was likely due to the influence of snowmelt. The sea-ice at Sta. #41 was the warmest that we encountered, and had relatively high S compared to the nearby stations. The elevated ice temperature may have resulted from the thin snow cover (3 cm; Table 1), which would have led to increased solar heating at the end of December. In addition, air and seawater temperatures were higher (−1.9 and −1.3°C, respectively), compared to water temperatures in the Amundsen Sea that were nearly close to the freezing point.

[23] The average brine temperature and standard deviation was −2.1 ± 0.4°C, with the coldest brine found at Sta. #13 (Table 2a). Brine salinity varied between 33.0 and 43.3, with the highest salinity also at Sta. #13. UIW temperature varied between −1.8°C (Sta. #1 and #21) and 0.4°C (Sta. #41), and salinity was approximately 33.4 at all stations (Table 2b).

4.1.2. Variability of Total Alkalinity and Dissolved Inorganic Carbon

[24] A_T varied between 123 and 800 μmol kg^{-1} (found at the bottom of the ice core at #18; Figure 5a), and the mean and standard deviation was 295 ± 107 μmol kg^{-1}. DIC ranged from 83 to 769 μmol kg^{-1}, with the mean of 273 ± 103 μmol kg^{-1}. At all stations, except Sta. #40 and #41, low DIC was found at mid-depths (30 to 130 cm) of the core, corresponding to the lower salinities there. The lowest DIC of 83 μmol kg^{-1} was found from 40 to 60 cm at Sta. #21 (Figure 5b), and the highest DIC at the same depth was found at Sta. #41. At the ice surface, the highest DIC (greater than 500 μmol kg^{-1}) was observed at Sta. #16, #21, #27 and #36. A_T was generally highest in the top 10 to 20 cm of the ice core, and lowest values at mid-depth, similarly to sea-ice salinity.

[25] In the brine, A_T varied between 2201 μmol kg^{-1} (Sta. #18) and 2932 μmol kg^{-1} (Sta. #13), and DIC between 1451 μmol kg^{-1} (Sta. #21) and 2204 μmol kg^{-1} (Sta. #36, Table 2a). In the UIW, the lowest A_T in the UIW was approximately 2275 μmol kg^{-1} (Sta. #35, #36, #41), and the highest A_T of 2368 μmol kg^{-1} was found at Sta. #1, along with the highest DIC of 2282 μmol kg^{-1}, which could be an effect of upwelling of Circumpolar Deep Water at the ACC (Table 2b). Except for Sta. #1, the highest A_T (2296 μmol kg^{-1}) in the UIW was found at Sta. #21, coinciding with the lowest DIC of 2125 μmol kg^{-1}.

4.1.3. Variability of Inorganic Nutrients

[26] Phosphate concentrations ranged in the ice cores from 0 to 2.4 μmol L^{-1}, with the highest values at Sta. #1, which was located furthest from the coast and the polynya. From

Figure 5. Variability in the sea-ice core (cm) of (a) total alkalinity (A_T, μmol kg^{-1}), (b) total inorganic carbon (DIC, μmol kg^{-1}), (c) phosphate (PO_4, μmol L^{-1}), (d) nitrate (NO_3, μmol L^{-1}), (e) silicic acid ($Si(OH)_4$, μmol L^{-1}), and (f) chlorophyll a (chl, μg L^{-1}), from station #1 (distance 0 km, right end) to station #41 (left end). The black dots show the sampling depths at each station. Station numbers are shown in top of the plot with reference to Figure 1 and Table 1 for location.

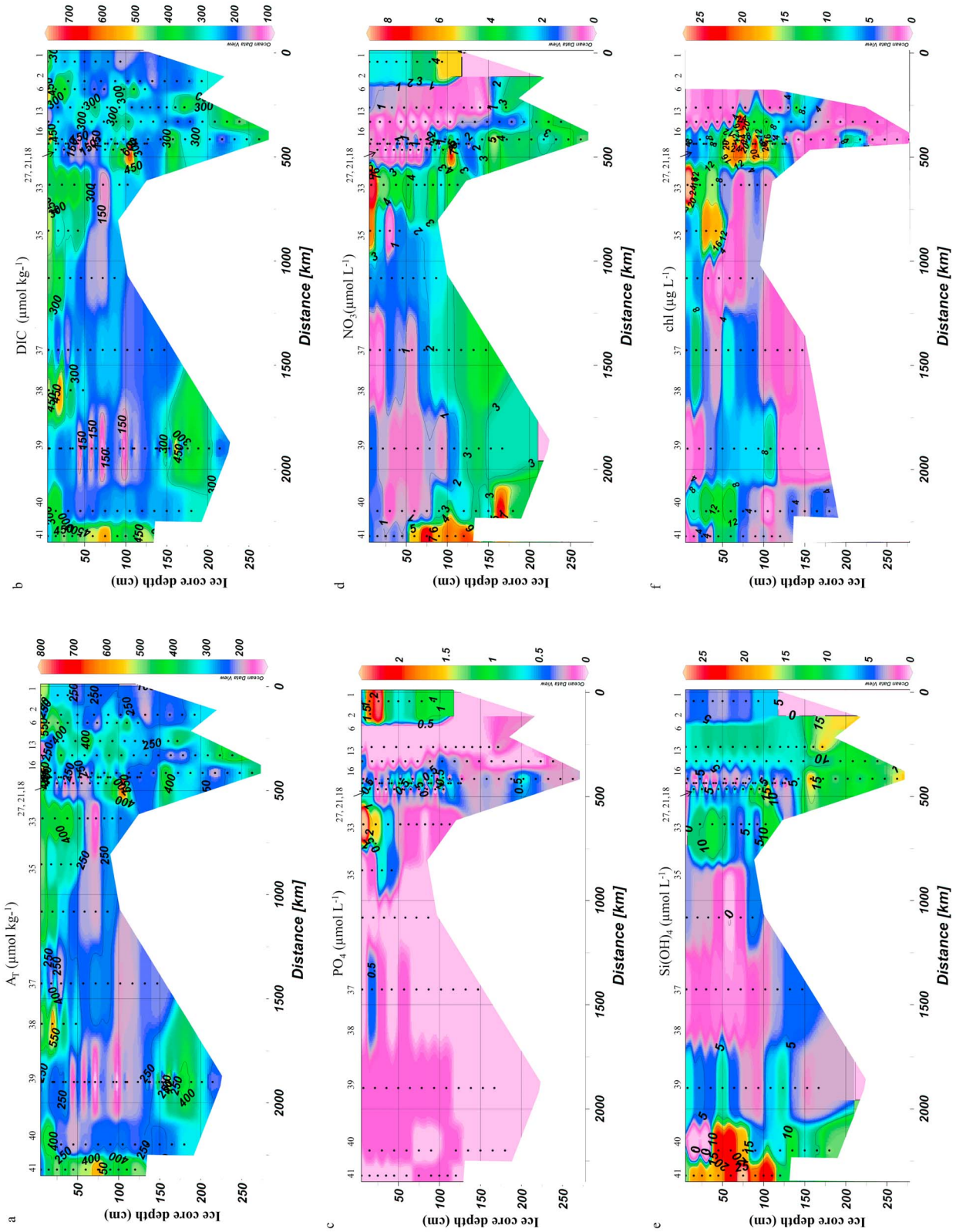
a
A_T (µmol kg^{-1})
b
DIC (µmol kg^{-1})
c
PO_4 (µmol L^{-1})
d
NO_3(µmol L^{-1})
e
$Si(OH)_4$ (µmol L^{-1})
f
chl (µg L^{-1})
Ice core depth (cm)
Distance [km]
27, 21, 18
Ocean Data View

Figure 5

Table 3. Average Concentrations and Standard Deviations of Phosphate (PO_4), Nitrate (NO_3), Silicic Acid ($Si(OH)_4$), Chlorophyll (chl), Particulate Organic Carbon (POC), and Particulate Organic Nitrogen (PON) in Sea Ice, Brine, and UIW[a]

Variable/ Sample	PO_4 (μmol L^{-1})	NO_3 (μmol L^{-1})	$Si(OH)_4$ (μmol L^{-1})	Chlorophyll (μg L^{-1})	POC (μmol L^{-1})	PON (μmol L^{-1})	POC:PON	POC:chl	Microbial Respiration (μmol C kg^{-1} d^{-1})
Ice	0.26 ± 0.43, N = 151 (0.0, 2.4)	2.1 ± 1.9, N = 151 (0.0, 8.7)	8 ± 6, N = 151 (0.0, 27)	14.9 ± 14.8, N = 52 0.83, 61.4)	184 ± 134, N = 52 30.3, 621)	19.6 ± 15.4, N = 52 2.23, 70.5)	9.39	148	12.8 ± 10.2, N = 10 1.74, 32.2)
Brine	0.25 ± 0.45, N = 9 0.0, 1.3)	3.5 ± 7.4, N = 9 0.0, 22.6)	17 ± 13, N = 9 5, 38)	2.71 ± 5.03, N = 11 0.02, 12.8)	20.8 ± 14.0, N = 11 2.92, 45.5)	2.48 ± 2.12, N = 11 0.34, 7.39)	8.36	91.8	2.05 ± 2.25, N = 8 0, 6.22)
UIW	1.5 ± 0.3, N = 13 0.7, 1.9)	27 ± 5, N = 13 16, 31)	57 ± 15, N = 13 37, 85)	4.31 ± 3.68, N = 8 0.26, 8.73)	18.1 ± 14.0, N = 8 1.98, 34.7)	3.30 ± 2.54, N = 8 0.37, 5.96)	5.50	50.4	2.09 ± 2.76, N = 12 0, 9.21)

[a]N is number of observations; values in parentheses are the minimum and maximum observed. POC:PON and POC:chl ratios represent the ratios of the means of each variable.

Sta. #36 to #41, the PO_4 concentrations were greatly reduced (less than 0.1 μmol L^{-1}) at all depths in the ice core, with a complete depletion at Sta. #13 (Figure 5c). Nitrate concentrations were also reduced from surface through 75 cm in the ice core at several locations (Figure 5d). At Sta. #16, #21 and #27, prominent NO_3 reductions from the surface to approximately 100 cm were observed. The highest NO_3 (8 μmol L^{-1}) was found at Sta. #33 in the top 10 cm and in the deeper part of the ice cores at the western-most stations (#40, #41). Silicic acid (Figure 5e) concentrations show similar variability as NO_3, with the highest values to the east and at the western-most station. Except for the western-most stations, $Si(OH)_4$ concentrations were higher toward the ice-water interface. However, at Sta. #40 and #41, we observed a prominent high-concentration feature at the mid-depth of the ice cores. Several stations showed $Si(OH)_4$ reductions in the upper 40 cm, and reduced values were found to about 150 cm depth at all stations east of Sta. #39.

[27] In the brine, nutrients showed large variability, with the highest concentrations at Sta. #18 (NO_3 of 23 μmol L^{-1}, PO_4 of 1.3 μmol L^{-1}, and $Si(OH)_4$ of 38 μmol L^{-1}, Table 3). Nutrients were depleted in the brine at Sta. #39, #40, and #41. At Sta. #21, PO_4 was depleted in the brine, and NO_3 and $Si(OH)_4$ were reduced as well (0.3 μmol L^{-1} and 11μmol L^{-1}, respectively). In the UIW nutrients were not depleted at any stations during sampling, with PO_4 greater than 1 μmol L^{-1} and NO_3 approximately 27 μmol L^{-1} (Table 3).

4.1.4. Variability of Pigments and Particulate Matter Concentrations

[28] Chlorophyll *a* within sea ice averaged 14.3 μg L^{-1} and ranged from 0.83–61.4 μg L^{-1} (Figure 5f and Table 3). Not all sections of all cores were analyzed for chlorophyll, and the assessed cores were likely biased toward those exhibiting color. Particulate organic carbon (POC) and nitrogen (PON) concentrations averaged 184 and 19.6 μmol L^{-1}, and ranged from 30.3–621 μmol C L^{-1} and 2.23–70.5 μmol N L^{-1}, respectively (Table 3). Despite the potential bias of sampling, a tremendous amount of variability was observed in all variables, which likely reflects the stage of temporal evolution of the ice algal assemblage. In contrast, brine and seawater 0.5 m under the ice (i.e., UIW) had mean chlorophyll concentrations of 2.71 and 4.31 μg L^{-1}, respectively, and POC and PON means of 20.8 and 2.48 μmol L^{-1} for brine, and 18.1 and 3.30 μmol L^{-1} for UIW (Table 3). POC:chl molar ratios averaged 9.39, 8.36 and 5.50 in ice, brine and UIW, suggesting that ice and brine had a substantial amount of detrital organic matter. This result was further confirmed by high C:chl ratios in ice, brine and seawater, averaging 148, 91.8 and 50.4 μg L^{-1}, respectively, indicating elevated amounts of non-autotrophic organic matter within the ice.

[29] Two accessory pigments were found in significant concentrations: 19′-hexanoyloxyfucoxanthin (19-hex) and fucoxanthin (fuco). The latter is characteristic of diatoms, and the average concentration found in sea ice was 2.63 ± 2.26 μg L^{-1} (range 0.07–7.62 μg L^{-1}). Average concentrations of 19-hex were less (1.08 ± 1.09 μg L^{-1}; range from non-detectable to 4.02). 19-hex is often associated with haptophytes such as *Phaeocystis antarctica*, but also is found in diatoms. The two were not significantly correlated, which may suggest they represented independent taxa. Unfortunately, no data are available for brine or underwater samples for comparison. Minor accessory pigment contributions were noted from peridinin (dinoflagellates) and chlorophyll c3. The latter pigment is often associated with haptophytes as well [*DiTullio et al.*, 2007], and in our samples was correlated with 19-hex (r^2 = 0.74), further suggesting a haptophyte origin.

4.1.5. Microbial Respiration

[30] Rates of dark CO_2 production by the microbial community were highest in the sea ice cores (ranging from 1.7–32.2 μmol C kg^{-1} d^{-1}), followed by UIW (ranging from not detectable to 9.2 μmol C kg^{-1} d^{-1}), with brine having the lowest rates (ranging from not detectable to 6.2 μmol C kg^{-1} d^{-1}). This was surprising since we expected much of the bacterial activity to be associated with the brine. Alternatively, with the high detrital content found in the ice (described above), bacteria likely attached to the particulate material in the ice channels and were not released into the brine when drained.

[31] The highest respiration rates in the ice cores tended to be weakly associated with warmer in situ temperatures (e.g., Sta. #35, #38, #40; r = −0.47, n = 9) and higher chlorophyll *a* concentrations (r = 0.55, n = 10), but correlated better with higher bacterial abundance (r = 0.72, n = 10) and higher POC and PON concentrations (r = 0.82 and 0.86, respectively). The highest respiration rates observed (32.2 μmol C kg^{-1} d^{-1}) were measured on a piece of brown "rotten ice" collected near Sta. 40 by a small boat. In general, the respiration rates measured in the pigmented layers of these ice

cores are comparable to rates measured similarly in productive surface waters of the coastal ocean.

[32] Despite relatively low levels, respiration rates in the less productive UIW correlated well with POC and PON concentrations (r = 0.78 and 0.81, respectively; n = 12), but not chlorophyll *a* (r = 0.02; n = 12). Dissolved organic carbon concentrations were fairly low in both the UIW and the brine (35–85 μmol L^{-1}; E. Ingall, personal communication, 2009), so most microbial heterotrophy was likely particle-associated. In the brine, respiration was weakly associated (r = 0.42, n = 9) with dissolved organic nitrogen concentrations (0.3–14 μmol L^{-1}; E. Ingall, personal communication, 2009).

4.2. Controls of the Sea-Ice CO_2 System

[33] In sea ice, the processes involved in the CO_2-system dynamics are highly dependent on the physical characteristics of the sea ice. Thickness of the sea ice and snow, temperature, slush layer and occurrence and depth of freeboard, are all parameters that affect the transport of heat, brine, and likely influence gas exchange [*Ackley and Sullivan*, 1994; *Perovich et al.*, 2004; *Tison et al.*, 2008]. Sea-ice temperature affects the porosity of the sea ice, and the conditions for gas exchange [*Tison et al.*, 2008]. In winter, when the ice is cold, the porosity and brine volume percentage (BV) decreases [*Cox and Weeks*, 1983], with the result that gases are trapped within the ice. When ice warms, BV and porosity increase and at the limit of 5% BV, fluid and gas exchange are facilitated within the ice [*Golden et al.*, 1998, 2007; *Loose et al.*, 2009, 2010]. At most horizons in our late-spring and early summer ice cores, the BV was greater than 5% (data not shown), indicating that the sea ice was permeable to fluid and gas exchange. In addition, a stratified layer within the sea ice could affect the transport of gases within the ice [*Perovich et al.*, 2004]. Almost all ice stations had negative freeboard and the resulting slushy layers, which are highly permeable to gases (Table 1).

[34] Biological processes controlling the sea-ice CO_2 system, such as algal production and associated CO_2 drawdown, also tends to be driven by irradiance (and therefore snow cover) and brine volume. Non-biogenic precipitation of $CaCO_3$ in brine channels during sea-ice formation also affects CO_2 (equation (1)), and dissolution of $CaCO_3$ can occur during sea-ice melting. The ratio between A_T and DIC (A_T:DIC ratio) in UIW and in sea ice indicates $CaCO_3$ precipitation or dissolution within the ice. During $CaCO_3$ precipitation in sea ice, the A_T and DIC decreases in the brine, whereas the concentration of CO_2 (aqueous phase) increases [e.g., *Jones and Coote*, 1981; *Killawee et al.*, 1998; *Papadimitriou et al.*, 2004; *Rysgaard et al.*, 2007; *Dieckmann et al.*, 2008] according to equation (1):

$$Ca^{2+} + 2HCO_3^- \Leftrightarrow CaCO_3(s) + H_2O + CO_2(aq) \quad (1)$$

The excess CO_2 released during $CaCO_3$ precipitation, however, is more easily dissolved in the brine and transported with the brine from the ice to the UIW, than the $CaCO_3$ particles, which are trapped within the ice [e.g., *Rysgaard et al.*, 2007; *Dieckmann et al.*, 2008]. Consequently, the A_T:DIC ratio increases in the ice during $CaCO_3$ precipitation and decreases in the UIW below. The trend of A_T:DIC ratio in the UIW can be a particularly useful indicator of $CaCO_3$ precipitation or dissolution: a decreasing A_T:DIC ratio in the UIW and brine (compared to in the ice) indicates $CaCO_3$ precipitation in the sea ice, whereas increased A_T:DIC ratio in the UIW occurs during ice melt and $CaCO_3$ dissolution.

4.2.1. A Simple Box Model Approach to Estimate Contributions to Carbon Fluxes

[35] We investigated the biogeochemical controls on the variability of the sea-ice CO_2 system and changes in DIC using a simple box model approach. A similar approach was used previously [*Fransson et al.*, 2004] for carbon transformations in the water column in the Atlantic sector of the Southern Ocean to estimate the biological production, air-sea CO_2 fluxes, and their effects on the oceanic CO_2 system. For the calculations, we choose seven ice stations where the sea ice was less than 125 cm thick to allow comparison between similar types of ice (i.e. seasonal ice and not rafted). Figure 6 shows vertical depth-profiles of the parameters used in the box model from the seven stations. Although seawater and sea ice can advect independently, our approach assumes that the sea ice was formed from the winter water (Figure 3) directly below, and the concentrations at the depth of temperature minimum (T_{min}), and salinity of 34 were used to represent the remnant of the winter mixed layer [*Gordon and Huber*, 1990; *Fransson et al.*, 2004]. Table 4 summarizes the concentrations of temperature, salinity, A_T, DIC, PO_4, NO_3, A_T:DIC ratio for the WW at all seven stations. The averages and standard deviations on these parameters (Table 4) represent the uncertainty in the calculations due to our assumption.

[36] A theoretical inventory (C_{THEORY}), assuming a constant DIC and nutrient changes with salinity [*Thomas et al.*, 2010], was used in the box model to investigate the impact on sea-ice DIC of processes, other than salinity changes. We assumed a one-year period, covering sea-ice formation in austral autumn/winter 2008 (i.e., February/March; Figure 2) to melting conditions in austral summer (i.e. December 2008 and January 2009). C_{THEORY} was calculated from the DIC and salinity differences between the sea ice and the winter water (Table 4), representing the surface water at the time of ice formation (Table 4). The difference (δC) between C_{THEORY} and the sea-ice inventory (C_{ICE}) in each ice core was used to investigate the role of processes other than brine rejection that may have affected sea-ice inventory, according to equations (2)–(4). For the change of DIC inventory δC_{DIC}, processes such as biological production (primary production and respiration; δC_{BIO}), ice-air CO_2 gas exchange (δC_{EXCH}) and $CaCO_3$ precipitation/dissolution (δC_{CaCO3}) are estimated.

$$\delta C = C_{THEORY} - C_{ICE} \quad (2)$$

$$\delta C_{DIC} = \delta C_{BIO} + \delta C_{SUM} \quad (3)$$

$$\delta C_{SUM} = \delta C_{CaCO3} + \delta C_{EXCH} \quad (4)$$

The parameter C_{SUM} is the combined effect of the other processes affecting DIC, after subtracting the biological effect, δC_{BIO}, from δC_{DIC}. The δC_{BIO} was calculated using nutrients and a similar approach as for DIC.

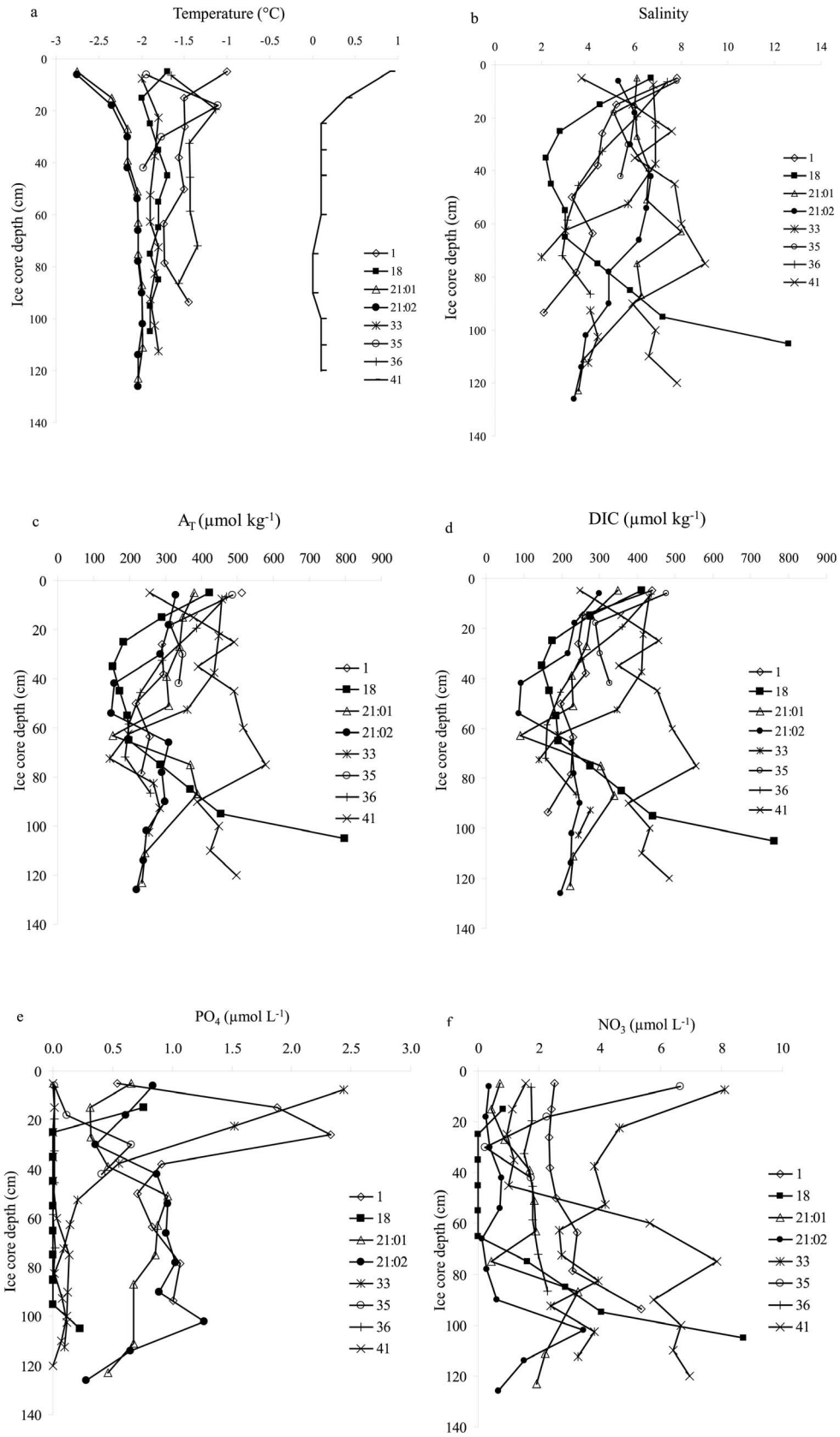

Figure 6. Vertical depth profiles in the sea ice of (a) temperature (°C), (b) salinity, (c) total alkalinity (A_T, μmol kg^{-1}), (d) total inorganic carbon (DIC, μmol kg^{-1}), (e) phosphate (PO_4, μmol L^{-1}), and (f) nitrate (NO_3, μmol L^{-1}) for the seven stations used in the model.

Table 4. Physical Properties of Depth, Temperature, and Salinity and Chemical Properties of Total Inorganic Carbon (DIC), Total Alkalinity (A_T), Phosphate (PO_4), Nitrate (NO_3), and Ratio of A_T and DIC (A_T:DIC Ratio) Found at the Depth of the Winter Water (WW), as Defined by the Temperature Minimum (Tmin), for Each Station[a]

Station	Depth (m)	Tmin (°C)	Salinity	DIC (μmol kg^{-1})	A_T (μmol kg^{-1})	PO_4 (μmol L^{-1})	NO_3 (μmol L^{-1})	A_T:DIC
1	50	−1.75	33.92	2196	2284	2.1	31	1.04
18	100	−1.79	34.02	2189	2297	2.2	26	1.05
21	100	−1.78	34.00	2197	2306	2.2	27	1.05
33	75	−1.83	34.04	2197	2303	2.2	28	1.05
35	70	−1.55	34.04	2201	2301	2.3	30	1.05
36	50	−1.63	34.03	2189	2295	1.5	n.d.	1.05
41	120	−1.80	34.07	2208	2306	1.8	n.d.	1.04
Average ± stdev	81 ± 27	−1.73 ± 0.10	34.02 ± 0.05	2197 ± 7	2299 ± 8	2.1 ± 0.3	28 ± 2	1.05 ± 0.1

[a]The average and standard deviation (stdev) for the parameters represent the uncertainty in the calculations due to the hypothesis of different location for ice formation and propagation of ice and seawater in the area.

[37] Production of DIC and nutrients occurs during respiration. In general, nutrients and iron are not limiting factors for primary production in sea ice, since sea ice is concentrated in nutrients and is considered to be a source of iron [e.g., *Lannuzel et al.*, 2007, 2008, 2010]. Several studies found higher concentrations of limiting nutrients within the sea ice, which may have implications for the primary production both within the sea ice, and in Antarctic waters [e.g., *Lannuzel et al.*, 2007]. A recent study in the Weddell Gyre in East Antarctica showed large primary production associated with sites of intense melting of sea ice and icebergs. This meltwater provided elevated iron concentrations to the surface water and fuelled an intense phytoplankton bloom [*Geibert et al.*, 2010].

[38] Assuming PO_4 and NO_3 as proxies for biological production, δC_{BIO} was calculated. The change in both PO_4 and NO_3 concentrations was converted to carbon equivalents using the classical RKR ratio of carbon to phosphate (C:P) ratio of 106 (106:1) and carbon to nitrate (C:N) ratio of 6.625 (106:16) by *Redfield et al.* [1963]. For comparison with the classical RKR ratio, we also used the POC:PON of 9.39 obtained from our data (Table 3). Using NO_3 and PO_4 as proxies for biological processes may add uncertainty to the DIC change, since NO_3 may be transformed into gaseous nitrogen during denitrification in sea ice [*Rysgaard and Glud*, 2004; *Rysgaard et al.*, 2008], and phosphorous may be precipitated in the sea ice [e.g., *Assur*, 1958].

4.2.2. Carbon Losses From the Sea Ice

[39] Table 5 summarizes the DIC inventory and the effects due to biological production, combined processes (δC_{SUM}), and brine rejected DIC (C_{BR}) from the seven ice stations of the Amundsen Sea and Ross Sea. According to the model, 80 to 90% of the salt 0.8 and 2.6 mol m^{-2} yr^{-1} (9.6 and 31 g C m^{-2} yr^{-1}) of DIC was rejected from the ice by the process of brine rejection. The gravity-driven brine rejection is the most efficient transport of DIC from the sea ice to the water column, whereupon the highly saline and cold surface water will sink to depths with equal density. All of the stations show positive δC_{DIC} indicating losses of DIC from the ice, from winter to summer, and positive δC_{DIC} losses. The largest δC_{DIC} was 0.14 mol m^{-2} yr^{-1} (1.7 g C m^{-2} yr^{-1}) for the duplicate sea-ice cores at Sta. #21, where δC_{DIC} was an order of magnitude larger than for other ice cores.

4.2.3. Net Biological Production

[40] Using NO_3 as proxy, all stations exhibited positive δC_{BIO} values and DIC losses from the ice due to net primary production. Since, no relationship between δC_{BIO} and algal biomass/particulate organic matter was observed, DIC was likely consumed in the ice during primary production, and the organic matter released later in summer from the ice to the surface water with the rejected brine or meltwater. The δC_{BIO} was positive for five stations, with the largest net DIC loss at Sta. #21, indicating relatively large (0.02–0.03 mol m^{-2} yr^{-1}, 0.24–0.36 g C m^{-2} yr^{-1}) net primary production. Sta. #21 had high particulate organic carbon and chlorophyll concentrations (averaging 225 μmol L^{-1} and 14.0 μg L^{-1}, respectively), suggesting that the biological processes contributed substantially to the reduced DIC. Using PO_4 as proxy, positive δC_{BIO} was obtained for three stations (#35, #36 and #41), with the largest DIC loss (0.04 mol m^{-2} yr^{-1}, 0.48 g C m^{-2} yr^{-1}) at Sta. #41, and negative δC_{BIO} for four

Table 5. Annual Sea-Ice Inventory of DIC Change (mol m^{-2} yr^{-1}), δC_{DIC}, and the DIC Change Due to Brine Rejection, δC_{BR}, Change in Organic-Matter Production Based on Changes in Phosphate (PO_4, P) and Nitrate (NO_3, N) Converted to Carbon Equivalents, $\delta C_{BIO(P)}$ and $\delta C_{BIO(N)}$, Where $\delta C_{BIO(P)}$ is Biological Production Based on the Carbon:Phosphate (C:P) Ratio of 16 [*Redfield et al.*, 1963][a]

Station	δC_{BR}	δC_{DIC}	$\delta C_{BIO(P)}$	$\delta C_{BIO(N1)}$	$\delta C_{BIO(N2)}$	$\delta C_{SUM(P)}$	$\delta C_{SUM(N1)}$	$\delta C_{SUM(N2)}$
1	2.6	0.03	−0.08	0.01	0.01	0.11	0.02	0.02
18	2.0	0.01	0.02	0.01	0.02	−0.01	0.00	−0.01
21*	1.9	0.14	−0.03	0.02	0.03	0.17	0.12	0.11
33	2.0	0.01	−0.04	0.00	0.00	0.05	0.01	0.01
35	0.8	0.02	0.01	0.01	0.01	0.01	0.01	0.01
36	1.6	0.03	0.02	n.d.	n.d.	0.01	n.d.	n.d.
41	1.9	0.03	0.04	n.d.	n.d.	−0.01	n.d.	n.d.

[a]$\delta C_{BIO(N1)}$ and $\delta C_{BIO(N2)}$ are biological production based on the carbon:nitrate (C:N) ratio of 6.625 [*Redfield et al.*, 1963] and POC:PON ratio (9.39) from this study, respectively. The $\delta C_{SUM(P)}$ and $\delta C_{SUM(N)}$ represent the DIC change caused by other processes, such as $CaCO_3$ precipitation/dissolution or CO_2 exchange. Asterisk denotes multiple ice cores, and n.d. means no data.

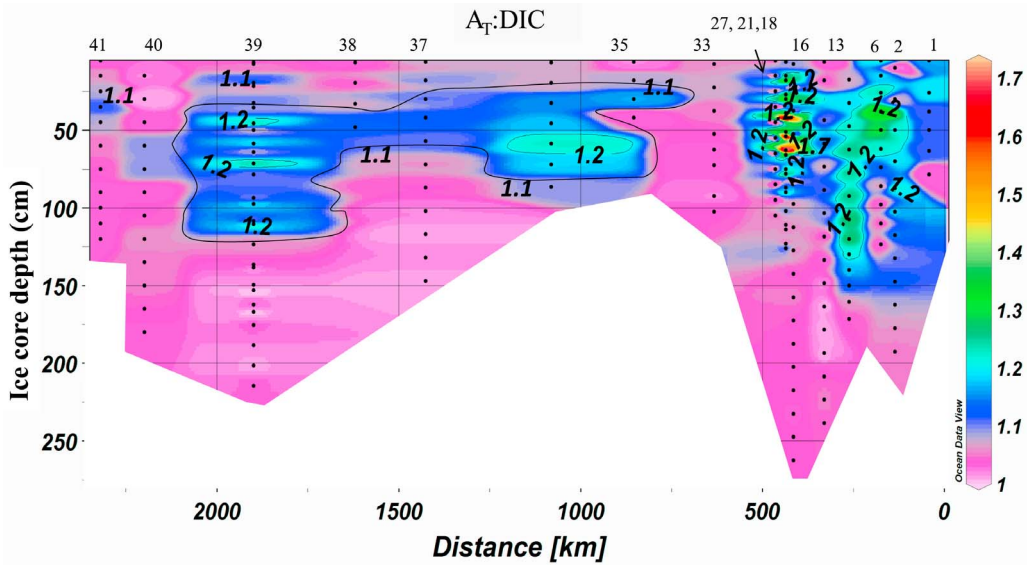

Figure 7. Variability in the sea-ice core (cm) of the total alkalinity (A_T) and total inorganic carbon (DIC) ratio (A_T:DIC ratio), from station #1 (distance 0 km, right end) to station #41 (left end). Station numbers are shown at the top of the plot with reference to Figure 1 and Table 1 for location.

stations (#1, #18, #21, #33), suggesting net heterotrophy. Station #21 showed both large net primary production and net heterotrophy, depending on the choice of proxies. With our approach, it is difficult to discern what proxy gives the most reliable representation of the biological processes (δC_{BIO}) in the sea ice during our study. Since the POC and chl were high at Sta. #21, and microbial respiration was modest, it is likely that NO_3 is a better proxy. Variations in δC_{BIO} (Table 5) for the different ice cores may be explained by differences in irradiance and nutrient availability. A deep snow layer, for example, would cause a significant reduction in available irradiance for primary production. At Sta. #33 (lowest net production) the snow layer was 60 cm compared to the much thinner snow layer (5 cm) at Sta. #21 where net production was greatest. Although depletion of nutrients is rarely observed in Antarctic sea ice [*Thomas et al.*, 2010], we observed depleted values of NO_3, PO_4 and even $Si(OH)_4$ in a number of ice cores (Figures 5c–5e). Hence, nutrients may have limited net biological production in some ice cores.

4.2.4. $CaCO_3$ Precipitation

[41] All but one station (#41) exhibited positive δC_{SUM} values, indicating a loss of DIC from the ice due to $CaCO_3$ precipitation and/or CO_2 outgassing from the ice (Table 5). The DIC gain at Sta. #41 (−0.01 mol m^{-2} yr^{-1}, −0.12 g C m^{-2} yr^{-1}) could have been due to CO_2 uptake during ice melt [e.g., *Nomura et al.*, 2010a]. This core was also the most saline, the warmest, the most nutrient depleted, and exhibited the largest biological CO_2 drawdown (using PO_4) compared to the other cores. In contrast, one of the colder cores (Sta. #21) showed the largest DIC loss (0.17 mol m^{-2} yr^{-1}, 2.04 g C m^{-2} yr^{-1}) to gas exchange or $CaCO_3$ precipitation. Since all ice cores experienced elevated A_T:DIC ratios (greater than 1.04) in the upper 65 cm, compared to the ratios in the UIW (Table 2b), with the highest A_T:DIC ratio in the ice of 1.7 at Sta. #21 (at 50 cm in core; Figure 7), we suspect solid $CaCO_3$ in the ice, dissolved during analysis. Moreover, the A_T versus salinity relationship, using all ice cores, showed that the core at Sta. #21 clearly deviated at 40–63 cm within the core (Figure 8a), where A_T was too low in relation to salinity. Remarkably, the highest A_T:DIC ratio of 1.6 and carbonate ion concentration ($[CO_3^{2-}]$) in the brine was found at Sta. #21 (Table 2a) and attributed to sea-ice $CaCO_3$ dissolution into the summer brine.

[42] Deviations from the typically good linear relationship between oceanic A_T and salinity in the UIW (Figure 8b) strongly suggest brine rejection and/or $CaCO_3$ dissolution into the surface ocean. Salinity normalized A_T in the UIW was higher in the UIW (2323 ± 12 μmol kg^{-1}) than in the WW (A_T = 2299 ± 8 μmol kg^{-1}), resulting in a difference of 24 μmol kg^{-1}. In addition, the $[CO_3^{2-}]$ in the UIW was highest at Sta. #21 (Table 2b), reflecting the precipitated $CaCO_3$, dissolved in the UIW during ice melt.

4.2.5. Gas Exchange

[43] Carbon losses from the ice due to gas exchange, at least during the season of our observations would seem unlikely. The fCO_2 values in the brine samples varied between 8 (Sta. #21) and 210 (Sta. #36) μatm, highly undersaturated with respect to the atmospheric level of approximately 380 μatm. We found elevated fCO_2 values (mean 414 ± 19 μatm) in the UIW at three stations (Table 2b), and undersaturated UIW at Sta. #21 (230 μatm), #27 and #33 (320 μatm). The higher fCO_2 values could be explained by the addition of CO_2-rich brine transported of out of the ice as the effect $CaCO_3$ precipitation and excess CO_2 within the sea ice. The low fCO_2 at Sta. #21, #27, and #33 in the UIW could be explained by the dissolution of $CaCO_3$, consuming CO_2 (especially at Sta.#21), during ice melt but also CO_2 uptake by primary production.

[44] For the DIC loss, another possible explanation could be CO_2 outgassing during previous freezing, where CO_2 escapes from the ice to the atmosphere. Experiments carried out by *Nomura et al.* [2006] during freezing of seawater, and field studies in the Arctic by *Rysgaard et al.* [2009] and

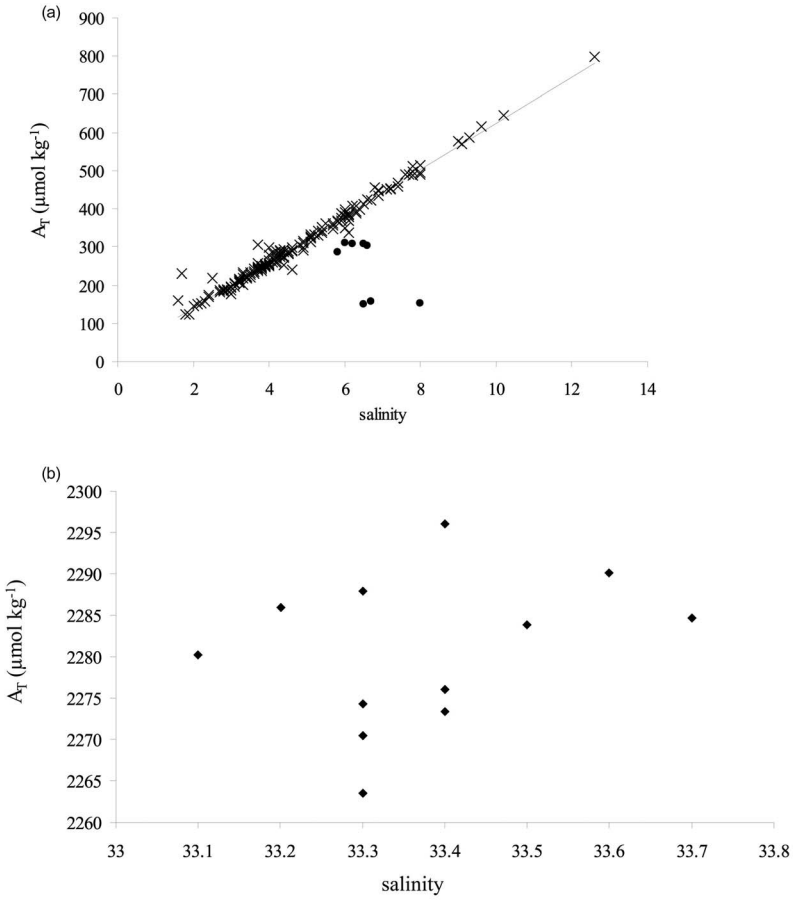

Figure 8. (a) The linear fit between total alkalinity (A_T) and salinity in the sea ice. Deviations from the line were found in the ice at #21 (black dots), which indicate the impact of processes other than salinity and biological production on A_T. These data were excluded in the linear fit ($A_T = 60.4 \times S + 18.8$, $r^2 = 0.98$, N = 188). (b) The linear fit between total alkalinity (A_T) and salinity in the under-ice water (UIW) showed no significant linear correlation ($r^2 = 0.09$, N = 12).

Miller et al. [2011], have shown an effect on air-sea CO_2 fluxes. However, this process is not fully understood and cannot be proved in this work.

4.2.6. Uncertainties

[45] One uncertainty of the model approach was the use of WW as the water of ice formation. During the ice season, sea ice is possibly affected by wind stress, wave actions and physical upwelling, causing movements of the ice floes.

[46] To investigate the uncertainty in the δC_{DIC} and δC_{BIO}, we used the full range of the WW concentrations (Table 4). We found that salinity the differences had no effect on the resulting δC_{DIC} or δC_{BIO}. The variability in WW DIC contributed to less than 20% to the δC_{DIC} estimates. The largest uncertainty was introduced by the variability of NO_3 and PO_4 on δC_{BIO}, resulting in an uncertainty of less than 30% and 60%, respectively. The large uncertainty in δC_{BIO} may be due to the fact that we did not account for recycled nutrients and differing C:P:N ratios, and other methods need to be used to ascertain the biological effect.

[47] The A_T:DIC ratio in the WW was approximately the same, 1.05, which suggests that, although the water or ice were moving, the uncertainty for the calculations of $CaCO_3$ precipitation was minimized. Uncertainty due to mixing and upwelling of CDW during austral summer could affect the water, hence the ice properties.

4.3. Effect of Sea-Ice Melt on the Mixed Layer and the Uptake of Atmospheric CO_2

[48] During ice melt in spring and summer, the A_T:DIC ratio becomes higher in the ice melt, than in the UIW, caused by the previously rejected CO_2. Therefore, CO_2 uptake from the surrounding water or atmosphere might be expected. Assuming two scenarios; one where there is no $CaCO_3$ precipitation and A_T:DIC ratio of 1.0; and another where the only impact on DIC results from sea-ice $CaCO_3$ precipitation and the A_T:DIC of 1.7. The difference between the two scenarios gives an indication on the increased potential for uptake of atmospheric CO_2 due to the process of $CaCO_3$ precipitation in the ice and dissolution during melt, in combination with brine rejection.

[49] We used the seven ice stations (used in the model) for the averages of the WW (Table 4) salinity (34.0), temperature (−1.5°C), DIC (2197 μmol kg^{-1}) and A_T (2299 μmol kg^{-1}). For the scenario of A_T:DIC ratio of approximately 1.0, we used the averages of sea ice salinity (4.6), temperature (−1.7°C), DIC (273 μmol kg^{-1}) and A_T (293 μmol kg^{-1}) at the time of melting in December/January. For the scenario

of A_T:DIC ratio of 1.7, we adjusted the sea-ice DIC (175 μmol kg^{-1}) to obtain the right ratio. We assumed addition of meltwater from sea ice (20 m thick layer) on top of the mixed surface layer (61 m), resulting in total mixed layer of 81 m (average winter water depth), in a similar approach used by *Rysgaard et al.* [2007]. Since we used the sea-ice thickness of maximum 1.2 m, assumed as seasonal Antarctic sea ice, compared to 1.8 m in the Arctic sea-ice study by *Rysgaard et al.* [2007], we assumed the melt layer to be 20 m, instead of 30 m. Addition of meltwater and mixing of the whole mixed surface layer was assumed, resulting in the mixed salinity of 27, temperature of −1.1°C, DIC of 1722 μmol kg^{-1}, and A_T of 1804 μmol kg^{-1}. Using the CO2SYS program for the calculation of fCO_2 in the two scenarios, we obtained the fCO_2 values of 279 and 223 μatm, respectively. The fCO_2 difference of 56 μatm between the two scenarios was attributed to the increased potential for uptake of atmospheric CO_2 due to the combination of $CaCO_3$ precipitation in sea ice, brine rejection and sea-ice melt. The result is in close agreement with results of 60 μatm obtained by *Rysgaard et al.* [2007], and it reflects the importance of sea ice and $CaCO_3$ precipitation within the ice for the uptake of atmospheric CO_2.

5. Conclusion

[50] The sea-ice processes involved in the vertical carbon transport have been investigated in this work. Brine rejection clearly dominates the carbon fluxes between the sea ice and the ocean, but we have no estimate of the amount of inorganic carbon that is actually exported out of the mixed layer and sequestered in the deep water. Calcium carbonate precipitation and dissolution can also have a large impact, particularly on the UIW. The A_T:DIC ratios give the result of the effect, with no actual evidence of the occurrence of solid $CaCO_3$. Biological drawdown by net autotrophy can also contribute significantly to the carbon flux, especially when sea ice is warm and porous. Gas exchange cannot explain carbon losses from the ice during the summer. Summer sea ice and brine were both observed to have significantly undersaturated fCO_2 with respect to the atmosphere. Significant fluxes from the atmosphere into the ice would depend on ice permeability and would likely lead to an underestimate of other fluxes. Yet, these complex processes are still not fully understood. The question of CO_2 exchange during ice melt, promoting atmospheric CO_2 uptake needs to be further investigated.

[51] To improve the methods for studying sea-ice processes, we need elaborate analyses using models in combination with more field measurements, especially in fall/winter and early spring. Using in situ measurements with sensors would be of great advantage, as well as under-ice measurements of brine rejection. $CaCO_3$ measurements in ice samples and frost flowers would be preferable to estimate the amount of $CaCO_3$ precipitated in the ice and ejected.

[52] The importance of sea ice as the promoter of the CO_2 uptake of atmospheric CO_2 and the vertical carbon transport out of the mixed layer has been highlighted in climate change scenarios. In the scenario with less summer ice and more open water, the potential for direct CO_2 uptake may increase. Yet, we still do not know the relative importance of ice-covered oceans for direct CO_2 uptake. Perhaps the carbon transport due to the sea-ice processes of $CaCO_3$ precipitation, brine rejection and $CaCO_3$ dissolution has greater importance than the direct CO_2 exchange in open water.

[53] **Acknowledgments.** This work is a contribution to the Oden Southern Ocean Expedition 2008/09 funded by the Swedish science council (VR) projects: DNR 2008–6226, 2008–6228, and 2009–2994 and NSF grants ANT-0836112 and ANT-0836144 (Antarctic Organisms and Ecosystems Program). Ray Sambrotto generously provided us with the nutrient data. Jonathan Brett Heimlich skillfully ran the respiration and DIC samples at sea. We thank My Mattsdotter and Madeleine Nilsson for chemical analyses. We are grateful for the constructive and valuable comments from two anonymous reviewers. We are also grateful to the support by the Captain and crew on the Swedish icebreaker *IB Oden*, and the Swedish Polar Research Secretariat and Raytheon Polar Services for logistical and technical support.

References

Ackley, S. F., and C. W. Sullivan (1994), Physical controls on the development and characteristics of Antarctic sea ice biological communities—A review and synthesis, *Deep Sea Res.*, *41*, 1583–1604, doi:10.1016/0967-0637(94)90062-0.

Arrigo, K. R., and D. N. Thomas (2004), Large scale importance of sea ice biology in the Southern Ocean, *Antarct. Sci.*, *16*, 471–486, doi:10.1017/S0954102004002263.

Assur, A. (1958), Composition of sea ice and its tensile strength, in *Arctic Sea Ice, Publ. 598*, pp. 106–138, Natl. Res. Counc., Natl. Acad. of Sci., Washington, D. C.

Chierici, M., and A. Fransson (2009), $CaCO_3$ saturation in the surface water of the Arctic Ocean: Undersaturation in freshwater influenced shelves, *Biogeosciences*, *6*, 2421–2431, doi:10.5194/bg-6-2421-2009.

Chierici, M., A. Fransson, and L. G. Anderson (1999), Influence of m-cresol purple indicator additions on the pH of seawater samples: Correction factors evaluated from a chemical speciation model, *Mar. Chem.*, *65*, 281–290, doi:10.1016/S0304-4203(99)00020-1.

Chierici, M., A. Fransson, D. Turner, E. A. Pakhomov, and P. W. Froneman (2004), Variability in pH, fCO_2, oxygen and flux of CO_2 in the surface water along a transect in the Atlantic sector of the Southern Ocean, *Deep Sea Res., Part II*, *51*, 2773–2787, doi:10.1016/j.dsr2.2001.03.002.

Clayton, T. D., and R. H. Byrne (1993), Spectrophotometric seawater pH measurements: Total hydrogen ion concentration scale calibration of m-cresol purple and at-sea results, *Deep Sea Res., Part I*, *40*, 2115–2129.

Cox, G. F. N., and W. F. Weeks (1983), Equations for determining the gas and brine volumes in sea ice samples, *J. Glaciol.*, *29*, 306–316.

Delille, B., B. Jourdain, A. V. Borges, J.-L. Tison, and D. Delille (2007), Biogas (CO_2, O_2, dimethylsulfide) dynamics in spring Antarctic fast ice, *Limnol. Oceanogr.*, *52*, 1367–1379, doi:10.4319/lo.2007.52.4.1367.

Deming, J. (2010), Sea ice bacteria and viruses, in *Sea Ice*, edited by D. N. Thomas and G. S. Dieckmann, pp. 247–282, Blackwell Sci., Oxford, U. K.

Dickson, A. G. (1990), Standard potential of the reaction: AgCl(s)+O H_2(g) = Ag(s)+HCl(aq), and the standard acidity constant of the ion HSO_4 in synthetic seawater from 273.15 to 318.15 K, *J. Chem. Thermodyn.*, *22*, 113–127, doi:10.1016/0021-9614(90)90074-Z.

Dickson, A. G. (1993), The measurement of seawater pH, *Mar. Chem.*, *44*, 131–142, doi:10.1016/0304-4203(93)90198-W.

Dickson, A. G., C. L. Sabine, and J. R. Christian (2007), Guide to best practices for ocean CO_2 measurements, *Spec. Publ.*, *3*, North Pac. Mar. Sci. Organ., Sidney, B. C., Canada.

Dieckmann, G. S., et al. (1998), A compilation of data on sea ice algal standing crop from the Bellingshausen, Amundsen and Weddell Seas from 1983 to 1994, in *Antarctic Sea Ice: Biological Processes, Interactions and Variability*, *Antarct. Res. Ser.*, vol. 73, edited by M. P. Lizotte and K. R. Arrigo, pp. 85–92, AGU, Washington, D. C.

Dieckmann, G. S., G. Nehrke, S. Papadimitriou, J. Göttlicher, R. Steininger, H. Kennedy, D. Wolf-Gladrow, and D. N. Thomas (2008), Calcium carbonate as ikaite crystals in Antarctic sea ice, *Geophys. Res. Lett.*, *35*, L08501, doi:10.1029/2008GL033540.

DiTullio, G. R., N. Garcia, S. F. Riseman, and P. N. Sedwick (2007), Effects of iron concentration on pigment composition in *Phaeocystis antarctica* grown at low irradiance, *Biogeochemistry*, *83*, 71–81, doi:10.1007/s10533-007-9080-8.

Flato, G. M., G. J. Boer, W. G. Lee, N. A. McFarlane, D. Ramsden, M. C. Reader, and A. J. Weaver (2000), The Canadian Centre for Climate Modeling and Analysis global coupled model and its climate, *Clim. Dyn.*, *16*, 451–467, doi:10.1007/s003820050339.

Fransson, A., M. Chierici, L. G. Anderson, and R. David (2004), Transformation of carbon and oxygen in the surface layer of the eastern Atlantic sector of the Southern Ocean, *Deep Sea Res., Part II*, *51*, 2757–2772, doi:10.1016/j.dsr2.2001.12.001.

Gardner, W. D., M. J. Richardson, and W. O. Smith Jr. (2000), Seasonal build-up and loss of POC in the Ross Sea, *Deep Sea Res., Part II*, *47*, 3423–3449, doi:10.1016/S0967-0645(00)00074-6.

Gasol, J. M., and P. A. De Giorgio (2000), Using flow cytometery for counting natural planktonic bacteria and understanding the structure of planktonic bacterial communities, *Sci. Mar.*, *64*, 197–224.

Geibert, W., et al. (2010), High productivity in an ice melting hot spot at the eastern boundary of the Weddell Gyre, *Global Biogeochem. Cycles*, *24*, GB3007, doi:10.1029/2009GB003657.

Golden, K. M., S. F. Ackley, and W. I. Lytle (1998), The percolation phase transition in sea ice, *Science*, *282*, 2238–2241, doi:10.1126/science.282.5397.2238.

Golden, K. M., H. Eicken, A. L. Heaton, J. Miner, D. J. Pringle, and J. Zhu (2007), Thermal evolution of permeability and microstructure in sea ice, *Geophys. Res. Lett.*, *34*, L16501, doi:10.1029/2007GL030447.

Gordon, A. L., and B. A. Huber, (1990), Southern Ocean winter mixed layer, *J. Geophys. Res.*, *95*, 11,655–11,672.

Grasshof, K. (1999), *Methods of Seawater Analyses*, John Wiley, Weinheim, Germany, doi:10.1002/9783527613984.

Haraldsson, C., L. G. Anderson, M. Hassellöv, S. Hulth, and K. Olsson (1997), Rapid, high-precision potentiometric titration of alkalinity in the ocean and sediment pore waters, *Deep Sea Res., Part I*, *44*, 2031–2044, doi:10.1016/S0967-0637(97)00088-5.

Jacobs, S. S., H. H. Hellmer, and A. Jenkins (1996), Antarctic ice sheet melting in the southeast Pacific, *Geophys. Res. Lett.*, *23*, 957–960, doi:10.1029/96GL00723.

Jenkins, A., D. G. Vaughan, S. S. Jacobs, H. H. Hellmer, and J. R. Keys (1997), Glaciological and oceanographic evidence of high melt rates beneath Pine Island glacier, West Antarctica, *J. Glaciol.*, *43*, 114–121.

Johnson, K. M., A. E. King, and J. M. Sieburth (1985), Coulometric TCO_2 analyses for marine studies: An introduction, *Mar. Chem.*, *16*, 61–82, doi:10.1016/0304-4203(85)90028-3.

Johnson, K. M., J. M. Sieburth, P. J. le B. Williams, and L. Brändström (1987), Coulometric total carbon dioxide analysis for marine studies: Automation and calibration, *Mar. Chem.*, *21*, 117–133, doi:10.1016/0304-4203(87)90033-8.

Jones, E. P., and A. R. Coote (1981), Oceanic CO_2 produced by the precipitation of $CaCO_3$ from brines in sea ice, *J. Geophys. Res.*, *86*(C11), 11,041–11,043.

Junge, K., H. Eicken, and J. W. Deming (2004), Bacterial activity at −2 to −20°C in Arctic wintertime sea ice, *Appl. Environ. Microbiol.*, *70*, 550–557, doi:10.1128/AEM.70.1.550-557.2004.

Killawee, J. A., I. Fairchild, J.-L. Tison, L. Janssens, and R. Lorrain (1998), Segregation of solutes and gases in experimental freezing of dilute solutions: Implications for natural glacial systems, *Geochim. Cosmochim. Acta*, *62*, 3637–3655, doi:10.1016/S0016-7037(98)00268-3.

Lannuzel, D., V. Schoemann, J. de Jong, J. L. Tison, and L. Chou (2007), Distribution and biogeochemical behavior of iron in the East Antarctic sea ice, *Mar. Chem.*, *106*, 18–32, doi:10.1016/j.marchem.2006.06.010.

Lannuzel, D., V. Shoemann, J. de Jong, L. Chou, B. Delille, S. Becquevort, and J. L. Tison (2008), Iron study during a time series in the western Weddell pack ice, *Mar. Chem.*, *108*, 85–95, doi:10.1016/j.marchem.2007.10.006.

Lannuzel, D., V. Schoermann, J. de Jong, B. Pasquer, P. van der Merwe, F. Masson, J. L. Tison, and A. Bowie (2010), Distribution of dissolved iron in Antarctic sea ice: Spatial, seasonal, and inter-annual variability, *J. Geophys. Res.*, *115*, G03022, doi:10.1029/2009JG001031.

Le Quéré, C., et al. (2007), Saturation of the Southern Ocean CO_2 sink due to recent climate change, *Science*, *316*, 1735–1738, doi:10.1126/science.1136188.

Lewis, M. J., J. L. Tison, B. Weissling, B. Delille, S. F. Ackley, F. Brabant, and H. Xie (2010), Sea ice and snow cover characteristics during the winter-spring transition in the Bellingshausen Sea: An overview of SIMBA 2007, *Deep Sea Res., Part II*, *58*(9–10), 1019–1038, doi:10.1016/j.dsr2.2010.10.027.

Lizotte, M. P. (2003), Microbiology of sea ice, in Sea Ice—An Introduction to Its Physics, Chemistry, Biology and Geology, edited by D. N. Thomas and G. S. Dieckmann, pp. 184–210, Blackwell Sci., Oxford, U. K.

Loose, B., W. R. McGillis, P. Schlosser, D. Perovich, and T. Takahashi (2009), Effects of freezing, growth, and ice cover on gas transport processes in laboratory seawater experiments, *Geophys. Res. Lett.*, *36*, L05603, doi:10.1029/2008GL036318.

Loose, B., P. Schlosser, D. Perovich, D. Ringelberg, D. T. Ho, T. Takahashi, J. Richter-Menge, C. M. Reynolds, W. R. McGillis, and J.-L. Tison (2010), Gas diffusion through columnar laboratory sea ice: Implications for mixed-layer ventilation of CO_2 in the seasonal ice zone, *Tellus, Ser. B*, *63*, 23–29, doi:10.1111/J.1600-0889.2010.00506.x.

Malmgren, F. (1927), *On the Properties of Sea Ice. The Norwegian North Polar Expedition With the "Maud", 1918–1925, Scientific Results*, vol. I, no. 5, Geofys. Inst., Univ. of Bergen, Bergen, Norway.

Manabe, S., R. J. Stouffer, and M. J. Spelman (1994), Response of a coupled ocean-atmosphere model to increasing atmospheric carbon dioxide, *Ambio*, *23*, 44–49.

Miller, L. A., et al. (2002), Carbon distributions and fluxes in the North Water, 1998 and 1999, *Deep Sea Res., Part II*, *49*, 5151–5170, doi:10.1016/S0967-0645(02)00183-2.

Miller, L. A., T. N. Papakyriakou, R. E. Collins, J. W. Deming, J. K. Ehn, R. W. Macdonald, A. Mucci, O. Owens, M. Raudsepp, and N. Sutherland (2011), Carbon dynamics in sea ice: A winter flux time series, *J. Geophys. Res.*, *116*, C02028, doi:10.1029/2009JC006058.

Nitsche, F., S. S. Jabobs, R. D. Larter, and K. Gohl (2007), Bathymetry of the Amundsen Sea continental shelf: Implications for geology, oceanography, and glaciology, *Geochem. Geophys. Geosyst.*, *8*, Q10009, doi:10.1029/2007GC001694.

Nomura, D., H. Yoshikawa-Inoue, and T. Toyota (2006), The effect of sea-ice growth on air-sea CO_2 flux in a tank experiment, *Tellus, Ser. B*, *58*, 418–426.

Nomura, D., H. Eicken, R. Gradinger, and K. Shirasawa (2010a), Rapid physically driven inversion of the air-sea ice CO_2 flux in the seasonal landfast ice off Barrow, Alaska after onset of surface melt, *Cont. Shelf Res.*, *30*, 1998–2004, doi:10.1016/j.csr.2010.09.014.

Nomura, D., H. Yoshikawa-Inoue, T. Toyota, and K. Shirasawa (2010b), Effects of snow, snowmelting and refreezing processes on air-sea-ice CO_2 flux, *J. Glaciol.*, *56*(196), 262–270, doi:10.3189/002214310791968548.

Orr, J. C., et al. (2005), Anthropogenic ocean acidification over the twenty-first century and its impact on calcifying organisms, *Nature*, *437*, 681–686, doi:10.1038/nature04095.

Papadimitriou, S., H. Kennedy, G. Kattner, G. S. Dieckman, and D. N. Thomas (2004), Experimental evidence for carbonate precipitation and CO_2 degassing during sea ice formation, *Geochim. Cosmochim. Acta*, *68*, 1749–1761, doi:10.1016/j.gca.2003.07.004.

Papakyriakou, T., and L. A. Miller (2011), Springtime CO_2 exchange over seasonal sea ice in the Canadian Arctic Archipelago, *Ann. Glaciol.*, *52*(57), 215–224, doi:10.3189/172756411795931534.

Perovich, D. K., B. C. Elder, K. J. Claffey, S. Stammerjohn, R. Smith, S. F. Ackley, H. R. Krousee, and A. J. Gow (2004), Winter sea-ice properties in Marguerite Bay, Antarctica, *Deep Sea Res., Part II*, *51*, 2023–2039, doi:10.1016/j.dsr2.2004.07.024.

Pierrot, D., E. Lewis, and D. W. R. Wallace (2006), MS Excel Program developed for CO_2 system calculations, *Rep. ORNL/CDIAC-105*, Carbon Dioxide Inf. Anal. Cent., Oak Ridge Natl. Lab., U.S. Dep. of Energy, Oak Ridge, Tenn.

Redfield, A. C., B. H. Ketchum, and F. A. Richards (1963), The influence of organisms on the composition of seawater, in *The Sea*, vol. 2, edited by M. N. Hill, pp. 26–77, John Wiley, New York.

Roy, R. N., L. N. Roy, K. M. Vogel, C. Porter- Moore, T. Pearson, C. E. Good, F. J. Millero, and D. M. Campbell (1993), The dissociation constants of carbonic acid in seawater at salinities 5–45 and temperatures 0–45°C, *Mar. Chem.*, *44*, 249–267, doi:10.1016/0304-4203(93)90207-5.

Roy, R. N., L. N. Roy, K. M. Vogel, C. Porter-Moore, T. Pearson, C. E. Good, F. J. Millero, and D. M. Campbell (1994), Erratum for: The dissociation constants of carbonic acid in seawater at salinities 5–45 and temperatures 0–45°C, *Mar. Chem.*, *45*, 337.

Rysgaard, S., and R. N. Glud (2004), Anaerobic N_2 production in Arctic Sea ice, *Limnol. Oceanogr.*, *49*, 86–94, doi:10.4319/lo.2004.49.1.0086.

Rysgaard, S., R. N. Glud, M. K. Sejr, J. Bendtsen, and P. B. Christensen (2007), Inorganic carbon transport during sea ice growth and decay: A carbon pump in polar seas, *J. Geophys. Res.*, *112*, C03016, doi:10.1029/2006JC003572.

Rysgaard, S., R. N. Glud, M. K. Sejr, M. E. Blicher, and H. J. Stahl (2008), Denitrification activity and oxygen dynamics in Arctic sea ice, *Polar Biol.*, *31*, 527–537, doi:10.1007/s00300-007-0384-x.

Rysgaard, S., J. Bendtsen, L. T. Pedersen, H. Ramlöv, and R. N. Glud (2009), Increased CO_2 uptake due to sea ice growth and decay in Nordic Seas, *J. Geophys. Res.*, *114*, C09011, doi:10.1029/2008JC005088.

Semiletov, I. P., A. P. Makshtas, S.-I. Akasofu, and E. L. Andreas (2004), Atmospheric CO_2 balance: The role of Arctic sea ice, *Geophys. Res. Lett.*, *31*, L05121, doi:10.1029/2003GL017996.

Smith, W. O., Jr., and V. A. Asper (2001), The influence of phytoplankton assemblage composition on biogeochemical characteristics and cycles in the southern Ross Sea, Antarctica, *Deep Sea Res., Part I*, *48*, 137–161, doi:10.1016/S0967-0637(00)00045-5.

Smith, W. O., Jr., V. Asper, S. Tozzi, X. Liu, and S. E. Stammerjohn (2011), Continuous fluorescence measurements in the Ross Sea, Antarctica: Scales of variability, *Prog. Oceanogr.*, *88*, 28–45, doi:10.1016/j.pocean.2010.08.002.

Spreen, G., L. Kaleschke, and G. Heygster (2008), Sea ice remote sensing using AMSR-E 89 GHz channels, *J. Geophys. Res.*, *113*, C02S03, doi:10.1029/2005JC003384.

Stammerjohn, S. E., D. G. Martinson, R. C. Smith, X. Yuan, and D. Rind (2008), Trends in annual Antarctic sea ice retreat and advance and their relation to El Niño–Southern Oscillation and Southern Annual Mode variability, *J. Geophys. Res.*, *113*, C03S90, doi:10.1029/2007JC004269.

Stouffer, R. J., S. Manabe, and K. Ryan (1989), Interhemispheric asymmetry in climate response to a gradual increase of atmospheric CO_2, *Nature*, *342*, 660–662, doi:10.1038/342660a0.

Takahashi, T., et al. (2009), Climatological mean and decadal change in surface ocean pCO_2, and net sea-air CO_2 flux over the global oceans, *Deep Sea Res., Part II*, *56*, 554–577, doi:10.1016/j.dsr2.2008.12.009.

Thoma, M., A. Jenkins, D. Holland, and S. Jacobs (2008), Modelling Circumpolar Deep Water intrusions on the Amundsen Sea continental shelf, Antarctica, *Geophys. Res. Lett.*, *35*, L18602, doi:10.1029/2008GL034939.

Thomas, D. N., and G. S. Dieckmann (Eds.) (2010), *Sea Ice*, 2nd ed., 402 pp., Blackwell Sci., Oxford, U. K.

Thomas, D. N., S. Papadimitriou, and C. Michel (2010), Biogeochemistry of sea ice, in *Sea Ice*, 2nd ed., edited by D. N. Thomas and G. S. Dieckmann, pp. 425–467, Blackwell Sci., Oxford, U. K.

Tison, J. L., A. Worby, B. Delille, F. Brabant, S. Papadimitriou, D. Thomas, J. de Jong, D. Lannuzel, and C. Haas (2008), Temporal evolution of decaying summer first-year sea ice in the Western Weddell Sea Antarctica, *Deep Sea Res., Part II*, *55*, 975–987, doi:10.1016/j.dsr2.2007.12.021.

Tremblay, J.-E., and W. O. Smith Jr. (2007), Phytoplankton processes in polynyas, in *Polynyas: Windows to the World's Oceans*, edited by W. O. Smith Jr. and D. G. Barber, pp. 239–269, Elsevier, Amsterdam, doi:10.1016/S0422-9894(06)74008-9.

United Nations Educational, Scientific, and Cultural Organization (1996), Protocols for the Joint Global Ocan Flux Study (JGOFS) core measurements, vol. 24, Paris.

Yager, P. L., D. W. R. Wallace, K. M. Johnson, W. O. Smith Jr., P. J. Minnett, and J. W. Deming (1995), The Northeast Water Polynya as an atmospheric CO_2 sink: A seasonal rectification hypothesis, *J. Geophys. Res.*, *100*, 4389–4398, doi:10.1029/94JC01962.

M. Chierici, Department of Chemistry, Marine Chemistry, University of Gothenburg, SE-412 96 Göteborg, Sweden.

A. Fransson, Department of Earth Sciences, Oceanography, University of Gothenburg, Box 460, SE-405 30 Göteborg, Sweden. (agneta@gvc.gu.se)

W. O. Smith Jr., Virginia Institute of Marine Sciences, College of William and Mary, Gloucester Point, VA 23062, USA.

P. L. Yager, Department of Marine Sciences, University of Georgia, Athens, GA 30602, USA.